THE GEOLOGICAL SOCIETY OF AMERICA®

Mafic intrusions record mantle inputs and crustal thickness in the eastern Sierra Nevada batholith, California, USA

Madeline J. Lewis[1,2,†], Juliet R. Ryan-Davis[2], and Claire E. Bucholz[2]

[1]*Department of Earth, Atmospheric, and Planetary Sciences, Purdue University, 550 Stadium Mall Drive, West Lafayette, Indiana 47907, USA*

[2]*Division of Geological and Planetary Sciences, California Institute of Technology, 1200 East California Boulevard, Pasadena, California 91125, USA*

ABSTRACT

Contributions of heat and/or mass from mafic magmas are commonly invoked in models of voluminous granodiorite and andesite generation in magmatic and volcanic arcs worldwide. However, mafic intrusions are a volumetrically minor component in most arc batholiths. This is the case in the Sierra Nevada batholith, California, USA, where gabbro and diorite plutons are smaller and less abundant than the granitoid suites that make up the bulk of the batholith. Here, we constrain the timing and geochemistry of mafic intrusions in the Sierra Nevada batholith to assess the role of these compositions in arc batholith construction. Previous detailed studies on a limited number of mafic intrusions demonstrate that they formed penecontemporaneously with the felsic batholith, but there is a need for a broader survey of mafic plutons using modern geochronological techniques. New U-Pb zircon ages for 13 gabbro to diorite plutons and geochemistry from 17 mafic intrusions in the eastern Sierra Nevada batholith document two main episodes of mafic magmatism in the eastern Sierra Nevada batholith, from 168 Ma to 145 Ma and from 100 Ma to 89 Ma. These episodes overlap with the ages of granitoid plutons in the eastern Sierra Nevada batholith, including the Late Jurassic Palisade Crest and Late Cretaceous John Muir intrusive suites, in addition to other felsic plutons dated in the eastern Sierra Nevada batholith. Nonprimitive mineral compositions in the mafic bodies indicate that their parental magmas are the evolved products of mantle-derived basalts that first differentiated in the lower crust prior to ascent and crystallization in the upper crust. The presence of rocks with cumulate textures, as well as a wide range of bulk-rock compositions (SiO_2 wt% 38–64, Mg# 39–74), show that magmatic differentiation continued within each mafic body after intrusion into the upper crust. Sr/Y ratios in melt-like (i.e., non-cumulate) mafic samples suggest that the crustal thickness of the Sierra Nevada batholith was roughly 30 km in the Early Jurassic and increased to ~44 km by the Late Cretaceous. Concomitant intrusion of mafic melts along with voluminous granitoid plutons supports mantle melting as a major contributor of heat and magmatic volumes to the crust during construction of the eastern Sierra Nevada batholith.

INTRODUCTION

The mid- to upper crust of arcs and the upper continental crust are broadly felsic in composition (>65 wt% SiO_2; Rudnick and Gao, 2003; Jagoutz and Schmidt, 2013; Jagoutz and Kelemen, 2015); however, mafic magmas are required to provide mass and heat for felsic magma production. Partial melting, fractional crystallization, assimilation, magma mixing, or some combination of these processes have been demonstrated as possible ways to form the intermediate to felsic compositions of arc batholiths, and all require a component of mafic magmatism (e.g., Frost and Mahood, 1987; Sisson et al., 1996; Wenner and Coleman, 2004; Zeng, et al., 2005; Otamendi et al., 2009; Blatter et al., 2013; Nandedkar et al., 2014; Jagoutz and Klein, 2018; Müntener and Ulmer, 2018). Documenting the ages and geochemistry of mafic and felsic plutons in the same arc provides an avenue for understanding their genetic relationships.

The Sierra Nevada batholith in eastern California, USA, active from ca. 220 Ma to 80 Ma (e.g., Kistler et al., 1965; Stern et al., 1981; Chen and Moore, 1982; Bateman, 1992a; Saleeby et al., 2008; Lackey et al., 2008), is one of the most comprehensively studied paleo-continental arcs worldwide. While the Sierra Nevada batholith is dominated by intermediate to felsic plutons (i.e., granitoids), mafic magmatism in the upper crust of the Sierra Nevada batholith has long been documented on a variety of scales (Mayo, 1941; Bateman and Eaton, 1967; Frost, 1987). For example, on the smallest scale, abundant mafic enclaves are found within some granitoids of the Sierra Nevada batholith and are direct evidence of contemporaneous mafic and felsic intrusions (Dorais et al., 1990; Frost and Mahood, 1987; Reid et al., 1983). Dominantly mafic dikes associated with the Independence dike swarm (Chen and Moore, 1979; Glazner et al., 2008; Hopson et al., 2008) intrude Jurassic and older plutons throughout the central-eastern Sierra Nevada batholith. Most reported dike ages are between 151 Ma and 148 Ma; however, the ages of dikes classified as part of the Independence dike swarm span from 157 Ma to 139 Ma (Hopson et al., 2008). In addition, Coleman et al. (2000) reported several Cretaceous (95–89 Ma) dioritic dikes. Several larger, dominantly mafic complexes are present in the northern and western Sierra Nevada batholith, including the ca. 164 Ma Emigrant Gap composite pluton (Saleeby et al., 1989; Girty et al., 1993), the ca. 149.5 Ma Guadalupe Igneous Complex (Ratschbacher et al., 2018), the 126–114 Ma Stokes Mountain ring dike complex (Clemens-Knott and Saleeby, 1999), and the 170–145 Ma mafic bodies on the Kern Plateau (Sisson and Moore, 2010; Gevedon, 2013). Furthermore, the southernmost Sierra Nevada batholith contains extensive exposures of lower-crustal gabbros as part of the Bear Valley intrusive suite (Sams and Saleeby, 1988; Ross, 1989; Pickett and Saleeby, 1993, 1994; Klein and Jagoutz, 2021; Rezeau et al., 2021). These mafic complexes comprise broadly coeval cumulate and melt-like litholo-

Madeline J. Lewis https://orcid.org/0000-0001-7968-2822

[†]maddie@purdue.edu

GSA Bulletin;
published online 29 August 2023

https://doi.org/10.1130/B36646.1; 7 figures; 2 tables; 1 supplemental file.

gies with internal compositional variation ranging from (ultra-)mafic (dunite, clinopyroxenite, troctolite, gabbro, gabbronorite, and diorite) to felsic (tonalite, granodiorite, and granite) lithologies (James, 1971; Clemens-Knott and Saleeby, 1999; Putirka et al., 2014), which demonstrates that intrusion and differentiation of mantle-derived melts occurred in the lower and upper crust of the Sierra Nevada batholith.

Similarly, smaller volume (<25 km^2, and many <5 km^2) gabbro and diorite intrusions are widespread in the upper crust of the Sierra Nevada batholith (>50 bodies; Fig. 1, Table 1). Though these intrusions were originally thought to be mafic precursors to the silicic batholith (Mayo, 1941; Ross, 1985), many of them have been shown to be contemporaneous with silicic magmatism both through field relationships and U-Pb zircon geochronology (e.g., Frost and Mahood, 1987; Coleman et al., 1995; Sisson et al., 1996; Coleman and Glazner, 1997; Ratajeski et al., 2001; Holland et al., 2013; Lewis et al., 2021). Parental melts to these mafic bodies represent low-Mg, high-Al hydrous basaltic to andesitic melts that were emplaced in the upper crust (Sisson et al., 1996; Lewis et al., 2021; Rezeau et al., 2021). Similarly, the Late Jurassic Independence dike swarm is dominantly non-primitive, but mafic (<55 wt% SiO_2) in composition (though dikes range from basaltic to rhyolitic; Glazner et al., 2008). Ninety percent of dikes within the Sierra Nevada batholith analyzed by Glazner et al. (2008) have magnesium numbers ($Mg\# = Mg/[Mg + Fe^T]$) <60, which is significantly lower than that of primitive basalts (i.e, undifferentiated, mantle-derived with Mg#s of ~70). Thus, the Sierra Nevada batholith mafic intrusions most likely represent mantle-derived melts that have undergone variable degrees of fractional crystallization and/or crustal assimilation since extraction from the sub-arc mantle.

These mafic melts are a potential source of both heat and mass that may have contributed to granitoid production in the Sierra Nevada batholith. Differentiation of low-MgO basalts can produce a range of mafic and granitoid compositions observed in the Sierra Nevada batholith and other arc batholiths (Sisson et al., 2005; Jagoutz et al., 2009; Jagoutz, 2010; Blatter et al., 2013; Nandedkar et al., 2014; Lewis et al., 2021), and heat provided by mafic magmas can cause partial melting and recycling of preexisting plutons and country rock (Annen and Sparks, 2002; Zeng et al., 2005; Collins et al., 2016; Moyen, 2020). Mixing between felsic melts, generated by differentiation of mafic melts and/or assimilation of preexisting crust, and mafic mantle-derived melts can generate the diversity of compositions observed in the Sierra Nevada batholith (Reid et al., 1983; Frost and Mahood, 1987; Sisson et al., 1996; Wenner and Coleman, 2004).

Although mafic magmatic rocks are widespread throughout the Sierra Nevada batholith (cf. Fig. 1) and demonstrably important to our understanding of batholith formation in the Sierra Nevada, modern geochronological data from mafic intrusions are limited, thereby limiting our understanding of their contribution to the extensive existing chronologic framework of the silicic batholith. Published geochronological data for mafic intrusions in the Sierra Nevada batholith are summarized in Table 1, along with new geochronology presented in this study. Previously published U-Pb zircon ages (both single-grain and bulk zircon analyses) are available for seven mafic plutons from the eastern Sierra, 10 mafic plutons from the western Sierra, and six mafic plutons from the southern Sierra and the Emigrant Gap Complex in the northern Sierra. Previous work has identified both Cretaceous (n = 13, 128–91 Ma; Saleeby and Sharp, 1980; Coleman et al., 1995; Clemens-Knott and Saleeby, 1999; Ratajeski et al., 2001; Gevedon, 2013; Holland et al., 2013; Klein et al., 2021; Lewis et al., 2021) and Jurassic mafic intrusions (n = 10, 170–145 Ma; Frost and Mattinson, 1993; Bartley et al., 2007; Gevedon, 2013; Saleeby and Dunne, 2015; Clemens-Knott, 2016; Ratschbacher et al., 2018; Gevedon et al., 2021), and a single Triassic quartz diorite body (240 Ma; Saleeby and Dunne, 2015).

In this study, we expand the current knowledge of crystallization ages of mafic plutons (Table 1, and Table S1 in the Supplemental Material[1]) and adjacent silicic granitoids (Table 2) from the eastern Sierra Nevada batholith via new U-Pb zircon geochronology from thirteen mafic intrusions and seven granitoid plutons. These new ages, in combination with bulk-rock and mineral geochemistry from seventeen mafic bodies, allow us to explore the temporal and genetic relationship between mafic and felsic intrusions in the eastern Sierra Nevada batholith.

Regional Geology and Field Relationships

The locations and mapped areas of the mafic complexes are shown in Figure 1B. This mapping is based on U.S. Geological Survey (USGS) maps (Moore, 1963; Bateman, 1992b) and a compilation of other USGS geologic maps by the U.S. Forest Service (Elder and Reichert, 2010, and referenced geologic maps therein). Intrusions in the eastern Sierra Nevada batholith are exposed to upper crustal levels of 100–300 MPa pressures (Ague and Brimhall, 1988; Chapman et al., 2012) equivalent to depths of roughly 5–12 km. In our descriptions of field relationships, we refer to our new U-Pb zircon ages, which are described further in the results, as well as ages that were previously published, to keep field descriptions complete and coherent. Reported ages are error-weighted means of individual spot ages for each sample, and reported uncertainties are 2 sigma of acceptable single-grain ages in each sample. In the discussion, U-Pb zircon ages are synthesized on a regional scale.

Ages and Intrusive Suites of the Sierra Nevada Batholith

Intermediate to felsic plutons of the Sierra Nevada batholith have been comprehensively dated, initially by K-Ar and bulk U-Pb zircon methods, and more recently with single-grain U-Pb zircon methods (e.g., Kistler et al., 1965; Evernden and Kistler, 1970; Stern et al., 1981; Chen and Moore, 1982; Coleman and Glazner, 1997; Wenner and Coleman, 2004; Coleman et al., 2004). Recognized spatial patterns in the crystallization ages of plutons reflect where magmatism occurred over time within the batholith. Triassic plutons are essentially restricted to exposures in the easternmost parts of the batholith. Jurassic plutons are exposed along the eastern Sierra range front and in the foothills of the western Sierra, but rarely in the central part of the batholith. Cretaceous intrusions progressed generally from west to east over time, which suggests the migration of active magmatism in rough belts parallel to the arc inwards toward the continent (Stern et al., 1981; Chen and Moore, 1982). Other geochemical measures, such as radiogenic isotopes and whole-rock chemistry, have been variably interpreted to follow these spatiotemporal relationships (e.g., Evernden and Kistler, 1970; Kistler and Peterman, 1973; DePaolo, 1981; Chen and Moore, 1982; Kistler and Anderson, 1990; Lackey et al., 2008). Magmatism in the Sierra Nevada batholith was protracted throughout the Mesozoic, and source compositions were spatially variable, so the particular age and location of an individual pluton should be considered when contextualizing its geochemistry within the batholith.

In certain cases, plutons may be associated temporally, spatially, and geochemically, particularly in well-known, large Cretaceous sys-

[1]Supplemental Material. The Supplemental Figures include maps, thin section and zircon images, figures used to display geochronological data for individual samples, and additional bulk-rock chemistry plots. The Supplemental Tables give the GPS locations of our samples, as well as bulk-rock chemistry, mineral chemistry, and zircon isotopic data. Please visit https://doi.org/10.1130/GSAB.S.23152709 to access the supplemental material, and contact editing@geosociety.org with any questions.

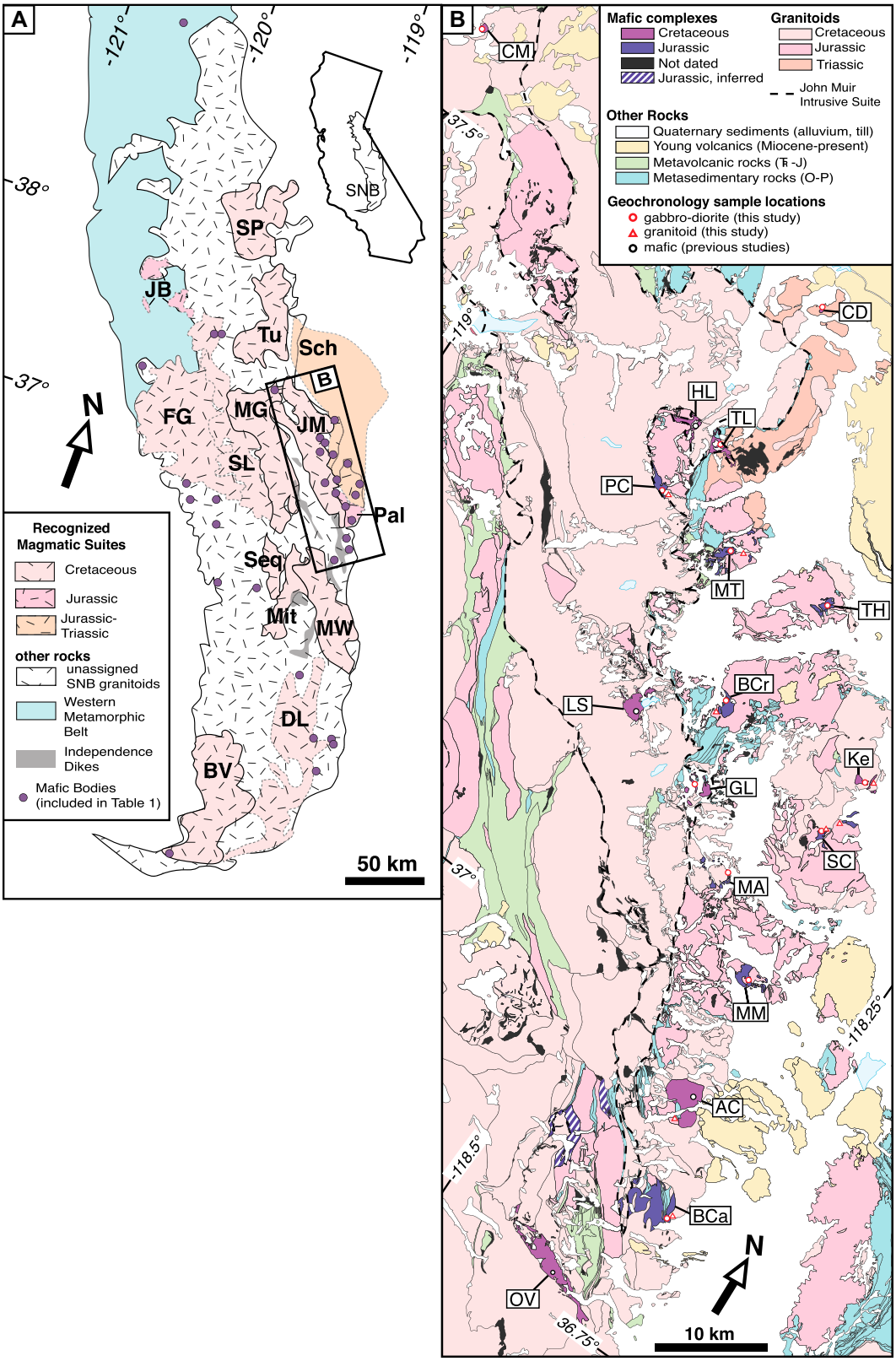

Figure 1. Simplified geologic maps of the Sierra Nevada batholith (SNB). (A) Overview of the Sierra Nevada batholith highlighting designated major magmatic suites and the extent of abundant dikes of the Independence dike swarm. Rectangle labeled B indicates the area of panel B. Magmatic suite abbreviations: SP—Sonora Pass; JB—Jawbone; Tu—Tuolumne; Sch—Scheelite; FG—Fine Gold; MG—Mount Givens; JM—John Muir; SL—Shaver Lake; Pal—Palisade Crest; Seq—Sequoia; Mit—Mitchell; MW—Mount Whitney; DL—Domelands; BV—Bear Valley. Suites with solid black outlines are nested intrusive suites, while those with dashed gray outlines are non-nested suites. Mapping and magmatic suites were adapted from Stern et al. (1981), Moore and Sisson (1987), Bateman (1992a), Hirt (2007), Lackey et al. (2008), Saleeby et al. (2008), Hildebrand (2013), Sisson and Moore (2013), and Frazer et al. (2014). Mafic bodies indicated by purple circles have existing geochronology (provided in Table S1; see text footnote 1) and are not meant to show all mafic bodies in the Sierra Nevada batholith. (B) Geologic map of the central-eastern Sierra Nevada batholith. Contacts are from Bateman (1992b) and a compilation by Elder and Reichert (2010). Mafic body abbreviations: CM—Cargyle Meadows; CD—Casa Diablo; HL—Hidden Lakes; TL—Tamarack Lakes; PC—Pine Creek: MT—Mount Tom; TH—Tungsten Hills; LS—Lake Sabrina; BCr—Bishop Creek; Ke—Keough; GL—Green Lake; SC—Shannon Canyon; MA—Mount Alice; MM—McMurry Meadows; AC—Armstrong Canyon; BCa—Black Canyon; OV—Onion Valley. The thick dashed line outlines the John Muir intrusive suite. Granitoid ages are from this study, Coleman et al. (1995), Lackey et al. (2008), Mahan et al. (2003), and Wenner and Coleman (2004). Several undated mafic bodies are inferred to be Jurassic or older, as they are intruded by the Jurassic Independence dike swarm (148 Ma; Chen and Moore, 1979).

TABLE 1. U-Pb ZIRCON AGES FOR DIORITE AND GABBRO BODIES OF THE SIERRA NEVADA BATHOLITH, CALIFORNIA

Mafic body	Abbrev.	Dated rock type	Sample	Latitude (°N)	Longitude (°W)	Age (Ma)	± (Ma)	Reference	Analytical method
Eastern Sierra									
Keough	Ke	Hb-diorite	SNB-18-53	37.2549	118.3961	88.8	1.3	This study	LA-ICP-MS
Cargyle Meadows	CM	Hb-gabbro	SNB-19-14	37.5719	119.1557	91.5	1.4	This study	LA-ICP-MS
Lake Sabrina	LS	Diorite	92TF105	[37.198]	[118.624]	91.1	0.3	Coleman et al. (1995)	ID-TIMS
Armstrong Canyon	AC	Diorite	AD-17	[36.959]	[118.356]	91.5	0.1	Coleman et al. (1995)	ID-TIMS
(Goodale, Aberdeen)		—	—	[36.959]	[118.356]	153.8*	1.5	Frost and Mattinson (1993)	Bulk zircon solution ICP-MS
Onion Valley	OV	Hb-plag segregations	IN93-18	[36.786]	[118.370]	92.1	0.3	Coleman et al. (1995)	ID-TIMS
Tamarack Lakes	TL	Equigranular amph-bt gabbro	SNB-18-13	37.4130	118.7120	94.6	1.1	This study	LA-ICP-MS
Hidden Lakes	HL	Monzodiorite	SNB-16-06	37.4107	118.7446	95.1	1	Lewis et al. (2021)	LA-ICP-MS
		Monzonite	SNB-16-09	37.4094	118.7446	95.6	0.8	Lewis et al. (2021)	LA-ICP-MS
		Quartz-monzodiorite	SNB-14-34	37.4176	118.7447	96.5	0.8	Lewis et al. (2021)	LA-ICP-MS
		Biotite-anorthosite	HL-17-02	37.4035	118.7438	95.7	0.7	Lewis et al. (2021)	LA-ICP-MS
		Monzodiorite	SNB-16-12	37.4073	118.7448	96.3	0.8	Lewis et al. (2021)	LA-ICP-MS
		Monzonite	SNB-14-40	37.4200	118.7510	90.5	0.8	Lewis et al. (2021)	LA-ICP-MS
Green Lake	GL	Amph-bt diorite	SNB-19-43	37.1711	118.5292	97.1	3.3	This study	LA-ICP-MS
Casa Diablo	CD	Medium-grained amph-gabbro	SNB-19-8	37.5501	118.7070	100.2	1.1	This study	LA-ICP-MS
Mount Tom	MT	Plag-rich gabbroic-diorite	SNB-19-16	37.3470	118.6369	145.1	1.7	This study	LA-ICP-MS
Mount Alice	MA	Amph-plag segregation	SNB-18-CB4	37.1252	118.4449	146.1	1.6	This study	LA-ICP-MS
Bishop Creek	BCr	bt gabbro	SNB-18-23	37.2417	118.5561	146.5	1.4	This study	LA-ICP-MS
Tungsten Hills	TH	Light, coarse, plag-rich diorite	SNB-19-34	37.3539	118.5257	148.3	1.8	This study	LA-ICP-MS
		Layered gabbro	12TH-3	37.3585	118.5282	151.2	0.7	Gevedon et al. (2021)	LA-ICP-MS
		—	—	[37.358]	[118.528]	150.3	1.5	Frost and Mattinson (1993)	Bulk zircon solution ICP-MS
McMurry Meadows	MM	Light, porphyritic amph-diorite	SNB-19-64	37.0648	118.3735	151.2	1.7	This study	LA-ICP-MS
		—	—	[37.065]	[118.371]	150.8	1.5	Frost and Mattinson (1993)	Bulk zircon solution ICP-MS
Black Canyon	BCa	Weakly foliated bt-diorite	SNB-19-23	36.8707	118.3038	157.2	2.4	This study	LA-ICP-MS
Shannon Canyon	SC	bt-rich diorite	SNB-19-52	37.2034	118.3996	168.2	1.9	This study	LA-ICP-MS
Pine Creek	PC	Light-colored diorite	SNB-19-60	37.3530	118.7312	194.0	2.6	This study	LA-ICP-MS
		Quartz diorite	—	37.3547	118.7292	97.5*	0.98	Frost and Mattinson (1988)	Bulk zircon solution ICP-MS
Southern Sierra									
Tunis Creek Gabbroids		Hb-rich gabbro	TM-15-49	34.9712	118.7721	100.196	0.085	Klein et al. (2021)	ID-TIMS
		Hb-rich gabbro	TM-15-75	34.9849	118.7626	100.064	0.033	Klein et al. (2021)	ID-TIMS
Osa Creek Ring Complex		Gabbro	—	[36.133]	[118.346]	146	1.5	Sisson and Moore (2010)	SHRIMP
Long Valley		Quartz monzodiorite	E12	35.8292	118.1119	148	1.5	Saleeby and Dunne (2015)	Bulk zircon ID-TIMS
Summit Gabbro		Hb gabbro	Fr-102	[36.093]	[118.110]	148–151	—	Gevedon (2013)	LA-ICP-MS
		Hb gabbro	Fr-103	[36.057]	[118.232]	148–151	—	Gevedon (2013)	LA-ICP-MS
		Gabbro	—	[36.093]	[118.110]	~150	—	Clemens-Knott (2016)	LA-ICP-MS
		Hb gabbro	E10	35.9389	118.0733	159	1	Saleeby and Dunne (2015)	Bulk zircon ID-TIMS
		Gabbro	JTRS032	35.8366	117.9741	168	10	Bartley et al. (2007)	SHRIMP
Sacatar Complex		Hb quartz diorite	E9	35.8558	117.9922	170	1	Saleeby and Dunne (2015)	Bulk zircon ID-TIMS
Walker Pass		Biotite-hb quartz diorite	E2	35.6644	118.0244	240	+8/–2	Saleeby and Dunne (2015)	Bulk zircon ID-TIMS
Western Sierra									
Windy Gap		Hb gabbro	KB10	[36.870]	[119.283]	98	—	Saleeby and Sharp (1980)	Bulk zircon solution ICP-MS
Yosemite (North America diorite)		Diorite	YOS-104	[37.731]	[119.633]	102	0.4	Ratajeski et al. (2001)	ID-TIMS
Yosemite (Rockslides)		Diorite	YOS-206	[37.723]	[119.666]	103	0.15	Ratajeski et al. (2001)	ID-TIMS
Ash Mountain		Gabbro	10JH20	36.5012	118.8129	105.1	0.9	Holland et al. (2013)	SHRIMP
		Gabbro	10JH18	36.5012	118.8129	105.5	0.7	Holland et al. (2013)	SHRIMP
Stokes Mountain		Gabbros	—	—	—	114–126	—	Gevedon (2013)	LA-ICP-MS
		Biotite-hb diorite dike	WBK134	36.4561	119.0764	117	2	Clemens-Knott and Saleeby (1999)	Bulk zircon ID-TIMS
Academy pluton		Quartz norite	KB4	[36.897]	[119.518]	120	—	Saleeby and Sharp (1980)	Bulk zircon solution ICP-MS
		Gabbro	8S02	36.9032	119.5061	118	1.6	Lackey et al. (2012)	LA-ICP-MS
Coyote Ridge		Gabbro	KB20	[36.824]	[119.436]	128	4	Saleeby and Sharp (1980)	Bulk zircon solution ICP-MS
Great Valley (from cores)		Hb-rich mafic cumulates	—	—	—	130–140	—	Saleeby (2007)	Bulk zircon
Guadalupe Igneous Complex		Amphibole gabbro	BRGIC13	37.4286	120.1677	149.504	0.038	Ratschbacher et al. (2018)	ID-TIMS
		Amphibole-dominated gabbro	BRGIC10	37.4094	120.1190	149.545	0.052	Ratschbacher et al. (2018)	ID-TIMS
		Pyroxene gabbro	BRGIC3	37.4741	120.1316	149.378	0.047	Ratschbacher et al. (2018)	ID-TIMS
Mill Creek		Hb quartz diorite	W2	36.7511	119.2174	169.5	1.5	Saleeby and Dunne (2015)	Bulk zircon ID-TIMS
Northern Sierra									
Emigrant Gap		Pyroxene quartz diorite	CC7	39.3000	120.5970	164	—	Saleeby et al. (1989)	Bulk zircon solution ICP-MS
		Two-pyroxene diorite	Sample A	39.3990	120.6260	163	4	Girty et al. (1993)	Bulk zircon ID-TIMS
		Two-pyroxene diorite	Sample B	39.3210	120.6380	164.5	0.5	Girty et al. (1993)	Bulk zircon ID-TIMS
Independence dikes									
Independence dikes (at Alabama Hills)		Silicic dikes associated with Independence dike swarm	—	[Alabama Hills, CA]		148	—	Chen and Moore (1979)	Bulk zircon solution ICP-MS
Independence dikes (at Woods Lake)		Diorite dike	WLT95-19	36.8911	118.3883	148	1	Coleman et al. (2000)	ID-TIMS
		Diorite dike	WLT94-10	36.8919	118.3733	94.4	0.7	Coleman et al. (2000)	ID-TIMS
Independence dikes, broadly		Diorite through granite dikes	[Sierra Nevada, White Mtns., Inyo Mtns., Coso Range, Benton Range, Mojave]			139–157	—	Hopson et al. (2008), compilation	Various

Note: Locations are given in brackets when no precise sample location is known. Instead, the latitude/longitude given indicates the location of the mafic body. Abbrev.—abbreviation; hb—hornblende; LA-ICP-MS—laser ablation–inductively coupled plasma–mass spectrometry; ID-TIMS—isotope dilution–thermal ionization mass spectrometry; plag—plagioclase; amph—amphibole; bt—biotite; SHRIMP—sensitive high-resolution ion microprobe; CA—California; Mtns.—Mountains.

*These dates disagree with newer data and use an older bulk zircon technique, so we prefer the more recent data collected via modern techniques, though we cannot rule out that the Pine Creek and Armstrong Canyon mafic bodies may be composite, containing both Jurassic and Cretaceous mafic intrusions.

TABLE 2. U-Pb AGES OF GRANITOIDS IN CONTACT WITH MAFIC BODIES IN THIS STUDY

Granitoid	In contact with mafic body	Sample	Latitude (°N)	Longitude (°W)	Age (Ma)	± (Ma)	Reference	Analytical method
King Creek Granodiorite	Cargyle Meadows	EH3-1	37.6289	119.1534	161.7–160.6	—	Tobisch et al. (2000)	Bulk zircon ID-TIMS
Mount Givens Granodiorite	Cargyle Meadows	MG10-01	37.5047	119.2873	95.9–95.0	—	Frazer et al. (2014)	ID-TIMS
Round Valley Peak Granodiorite	Hidden Lakes	RVP-2	37.4570	118.7336	88.8	0.2	Gaschnig (2005)	ID-TIMS
Lake Edison Granodiorite (Morgan Creek Mass)	Hidden Lakes, Tamarack Lakes, Pine Creek	07-MC-009	[37.371]	[118.731]	93.5	{1.9}	Porter (2013)	LA-ICP-MS
Granite of Chickenfoot Lake	Hidden Lakes, Pine Creek	SNB-18-02	37.3977	118.7553	191.78	2	Lewis et al. (2021)	LA-ICP-MS
Mono Creek Granite	Pine Creek	MC-1	37.4192	118.7708	87	0.1	Gaschnig (2005)	ID-TIMS
Quartz monzonite of Wheeler Crest	Casa Diablo, Tamarack Lakes	MT-10	37.4010	118.6574	207	{4.1}	Stern et al. (1981)	Bulk zircon ID-TIMS
Tungsten Hills Quartz Monzonite (at Mount Tom)	Mount Tom	SNB-19-21	37.3492	118.6295	201.0	2.6	This study	LA-ICP-MS
Tungsten Hills Quartz Monzonite (at Tungsten Hills)	Tungsten Hills	MT-11	37.3800	118.6796	201.9	{4.0}	Stern et al. (1981)	Bulk zircon ID-TIMS
Tungsten Hills Quartz Monzonite (at Bishop Creek)	Bishop Creek	SNB-18-45	37.2354	118.5611	167.8	1.6	This study	LA-ICP-MS
Tungsten Hills Quartz Monzonite (at Shannon Canyon)	Shannon Canyon	SNB-19-54	37.2049	118.3968	170.8	1.9	This study	LA-ICP-MS
Kca* (at Shannon Canyon)	Shannon Canyon, Green Lake	SNB-19-56	37.2150	118.3892	145.3	1.2	This study	LA-ICP-MS
Inconsolable Granodiorite	Green Lake	1S127	37.1224	118.4983	95	{1.9}	Lackey et al. (2008)	—
Lamarck Granodiorite	Green Lake, Lake Sabrina	MG-8	[37.169]	[118.567]	91.9	0.6	Coleman et al. (1995)	ID-TIMS
Leucogranite of Rawson Creek (at Keough)	Keough	SNB-18-52	37.2573	118.3861	97.2	1.1	This study	LA-ICP-MS
Leucogranite of Rawson Creek (at Big Pine Creek)	Mount Alice	BIc-1	37.2532	118.3785	95.3	{1.9}	Stern et al. (1981)	Bulk zircon ID-TIMS
Tinemaha Granodiorite	McMurry Meadows, Mount Alice	—	[37.08]	[118.29]	164	{3.3}	Bateman (1992a)	Bulk zircon solution ICP-MS
Granodiorite of McMurry Meadows	McMurry Meadows	Undated, cogenetic with McMurry Meadows mafic body					Bateman (1992a)	—
Granite of Goodale Mountain	Armstrong Canyon	GG3-93	[36.974]	[118.368]	91.5	0.1	Coleman et al. (1995)	ID-TIMS
Siberian pluton	Armstrong Canyon	Undated, mingled with Armstrong Canyon diorite					Coleman et al. (1995)	—
Mule Lake pluton (at Armstrong Canyon)	Armstrong Canyon, Black Canyon	SNB-17-4	36.9508	118.3465	158.4	1.5	This study	LA-ICP-MS
Spook pluton	Black Canyon, Armstrong Canyon	SNB-19-24	36.8716	118.3009	103.8	2.9	This study	LA-ICP-MS
McDoogle pluton	Black Canyon	KMR	36.8820	118.3595	94	4	Mahan et al. (2003)	ID-TIMS
McGann pluton	Black Canyon	Undated, cuts features in McDoogle Pluton					Moore (1963)	—
Dragon pluton	Onion Valley	OW34	[36.777]	[118.332]	103	{2.1}	Chen and Moore (1982)	Bulk zircon ID-TIMS
Bullfrog pluton	Onion Valley	OW4	[36.770]	[118.348]	103	{2.1}	Chen and Moore (1982)	Bulk zircon ID-TIMS

Note: Latitude/longitude given in brackets is estimated from sample locations on maps, but not given as exact coordinates in the references. Uncertainties in curly brackets were not given in references and were computed as 2% of the reported age. ID-TIMS—isotope dilution–thermal ionization mass spectrometry; LA-ICP-MS—laser ablation–inductively coupled plasma–mass spectrometry.

*Kca: "rocks similar to the Cathederal Peak alaskaite," as mapped by Bateman (1965).

tems that become progressively younger and more evolved toward their centers, such as the Tuolumne and Whitney intrusive suites (Bateman and Chappell, 1979; Hirt, 2007). Indeed, much of the Sierra Nevada batholith has been classified into intrusive suites (Figs. 1A and S1; see footnote 1), each of which is composed of multiple plutons intruded over <20 m.y. and interpreted by some authors to be part of an individual magmatic episode (Stern et al., 1981; Bateman, 1992a). Suites defined by their progressively younger and more evolved, nested nature (e.g., Evernden and Kistler, 1970; Bateman and Chappell, 1979; Sisson and Moore, 1984; Hirt, 2007) are marked by cogenetic relationships among plutons and represent a magmatic event, whereas some suites defined only by age and broad geographic region likely do not, but can, provide a framework for tracking the age and location of a series of plutons. The intrusive suites shown in Figure 1 consist of several (about two to seven) granitoid plutons each and range in overall exposed area from several hundred square kilometers to ~2000 km^2. "Unassigned" plutons are located between defined intrusive suites.

The designated intrusive suites that display a nested intrusive architecture that youngs inward or eastward (Sonora Pass, Tuolumne, John Muir, Mount Whitney, Mount Givens, Sequoia, and Mitchell) trend toward more evolved (higher SiO_2) lithologies over time (Stern et al., 1981; Moore and Sisson, 1987; Bateman, 1992a; Coleman et al., 2004; Hirt, 2007; Davis et al., 2012; Sisson and Moore, 2013; Frazer et al., 2014; Leopold, 2016). These nested suites have been interpreted to represent localized periods of enhanced magmatism in the upper crust that underwent magmatic focusing over time (e.g., Ardill et al., 2018). The lower crustal Bear Valley intrusive suite, though not younging inward or becoming more evolved over time, was dominantly emplaced over a relatively short period (101.5–100.1 Ma), and magmatic compositions are consistent with an internally cogenetic magmatic system. Thus, this suite is also interpreted to represent a localized period of enhanced magmatism (Klein and Jagoutz, 2021; Klein et al., 2021). The designated suites that do not have a consistent compositional, spatial, and temporal structure like the nested suites (Fine Gold, Shaver Lake, Jawbone, Palisade Crest, Domelands, and Scheelite) were designated in earlier publications based on similar ages of plutons in adjacent locations (Stern et al., 1981; Bateman, 1992a; Saleeby et al., 2008). Below, we summarize reported ages of suites that have been designated by previous authors, recognizing that the non-nested suites may represent interpreted plutonic groupings based on intrusive age and location rather than on genetic relationships.

The Triassic Scheelite intrusive suite is the oldest identified suite in the Sierra Nevada batholith, ranging from 226 Ma to 218 Ma in age (Barth et al., 2011) and interpreted by some to contain the Tungsten Hills Quartz Monzonite (ca. 200 Ma; Stern et al., 1981; Bateman, 1992a). The Jurassic Palisade Crest and Jawbone intrusive suites, both of which are not nested, intruded between 164 Ma and 160 Ma (Stern et al., 1981; Bateman, 1992a). The oldest Cretaceous intrusive suite, the Fine Gold intrusive suite, comprises plutons in the western Sierra Nevada batholith with ages of between 124 Ma and 105 Ma (Lackey et al., 2012). The plutons associated with this ~20 m.y. span and large footprint are not a single well-defined nested suite and were emplaced incrementally from

west to east in at least three internal belt-like domains roughly parallel to the Sierra Nevada crest (Lackey et al., 2012). This is the longest-lived suite (nearly 20 m.y. lifetime) and thus may or may not represent a single magmatic event, as all of the nested suites were each active for <10 m.y. It is possible that the Fine Gold intrusive suite as currently defined represents multiple nested suites or includes intrusions that were not associated with a nested, zoned suite. Subsequently, in the Cretaceous, arc magmatism shifted eastward through time, creating the Shaver Lake (sometimes split into Shaver Lake and Yosemite Valley intrusive suites), Sequoia, Mount Givens (also called Kaiser), and Mitchell intrusive suites between 105 Ma and 91 Ma (Stern et al., 1981; Moore and Sisson, 1987; Bateman, 1992a; Sisson and Moore, 2013; Frazer et al., 2014). The youngest and easternmost series of Cretaceous intrusive suites in the eastern Sierra Nevada batholith, the Sonora Pass, Tuolumne, John Muir (also called Mono Pass), Mount Whitney, and Domelands intrusive suites, intruded between 96 Ma and 83 Ma (Leopold, 2016; Coleman et al., 2004; Hirt, 2007; Saleeby et al., 2008; Davis et al., 2012). Smaller intrusive suites identified by Stern et al. (1981), including the Washburn, Merced Peak, and Buena Vista intrusive suites (all between 107 Ma and 90 Ma; Stern et al., 1981) may represent plutons that are not part of a larger suite or suites that were dissected, recycled, or otherwise overprinted by the larger and later Cretaceous suites. The age ranges of these suites are associated with two periods of widely documented magmatism (also called flare-ups) identified by previous studies in the Sierra Nevada batholith, which occurred during the Late Jurassic (170–148 Ma) and Late Cretaceous (105–87 Ma; Stern et al., 1981; Chen and Moore, 1982; Ducea, 2001; Paterson and Ducea, 2015; Chapman et al., 2021).

Evidence of mafic magmatism is present in all intrusive suites as well as associated with unclassified plutons, as mafic enclaves and discrete mafic plutons within and amongst felsic plutons, and along intrusive contacts between granitoid plutons. Mafic bodies are commonly adjacent to granitoids of roughly the same age, and they can be older than, younger than, or coeval with adjacent granitoids, which we describe in detail below. Intrusive contacts that show definitive age relationships between mafic and felsic lithologies of this study are largely obscured by talus or till, but they have been closely observed at the Armstrong Canyon, Lake Sabrina, Hidden Lakes, Onion Valley, Pine Creek, and Tamarack Lakes bodies. Margins between mafic intrusions and surrounding granitoids of similar age are often mingled, as in the Lake Sabrina diorite (91.1 Ma) and the Lamarck Granodiorite (91.9 Ma), and the Armstrong Canyon Complex (92.1 Ma) and the granite of Goodale Mountain (91.5 Ma; Coleman et al., 1995). Contacts between younger mafic complexes and older granitoids are commonly gradational over tens of centimeters, as in the Hidden Lakes gabbros (95.1 Ma; Lewis et al., 2021) and the granite of Chickenfoot Lake (191.8 Ma; Lewis et al., 2021) and the Tamarack Lakes body (94.6 Ma) and the quartz monzonite of Wheeler Crest (Fig. 2A; 207 Ma; Stern et al., 1981), which suggests that the process of remobilization or remelting of felsic material by mafic magmas occurs within the upper crust. In the Hidden Lakes, Onion Valley, and Shannon Canyon complexes, diabase dikes extend from the mafic body into the older surrounding granitoids. Where granitoids intrude mafic complexes that are significantly older, the contacts are sharp (Fig. 2B) or the mafic complex may be brecciated by the intrusion of younger granitoids, as in the Hidden Lakes mafic complex (95.1 Ma; Lewis et al., 2021) and Round Valley Peak Granodiorite (88.8 Ma; Lackey et al., 2008), and the Mount Alice Complex (146.2 ± 1.5 Ma; this study) and the leucogranite of Rawson Creek (ca. 95 Ma; Wenner and Coleman, 2004). Below are additional descriptions of the field relationships and petrology of the mafic complexes sampled and analyzed.

Cargyle Meadows

An unnamed and previously unmapped mafic body near Cargyle Meadows, which we use as its name, is a small (0.17 km^2), amphibole-rich diorite through gabbro body with a U-Pb zircon age of 91.5 ± 1.4 Ma (this study). The body consists mainly of coarse-grained amphibole-dominated gabbro with amphibole oikocrysts up to 1.5 cm, and rare yet notable euhedral pyrite crystals of up to 4 mm. Clinopyroxene cores some amphibole grains (Fig. S2; see footnote 1). Plagioclase is interstitial in the gabbros and dominates the rock volume in the amphibole-biotite diorite. The complex is surrounded by the 95 Ma Mount Givens Granodiorite (Frazer et al., 2014), and it may contact the ca. 161 Ma granodiorite of King Creek (Tobisch et al., 2000) beneath Quaternary talus to the south.

Casa Diablo

This small mafic body is located near the town of Aspen Springs, California, and has a mapped area of 0.19 km^2. Its small, rounded geometry as mapped suggests a stock-like intrusion into the quartz monzonite of Wheeler Crest (207 Ma; Stern et al., 1981). With an age of 100.2 ± 1.1 Ma (this study), this is the oldest Cretaceous mafic intrusion in this study. The body is poorly exposed; however, rubbly outcrops show a medium-grained amphibole-gabbro and coarse-grained olivine-gabbro containing cumulate patches (20–50 cm) of amphibole-bearing olivine websterite (Fig. S2). All samples from this locality are classified as cumulates based on texture and chemistry.

Hidden Lakes

The 96–95 Ma Hidden Lakes mafic complex (2.5 km^2), located within Little Lakes Valley, intrudes the 191.8 ± 4.2 Ma granite of Chickenfoot Lake (Lewis et al., 2021) and is intruded by the Round Valley Peak Granodiorite (88.8 Ma; Gaschnig, 2005) and the Morgan Creek mass of the Lake Edison Granodiorite (93.5 Ma; Porter, 2013). The body consists mainly of a medium- to fine-grained amphibole-biotite gabbro, though coarse-grained gabbros exist in lenses of up to 200 m wide. The eastern section of the complex displays a gradational transition from south to north of norite and gabbro cumulates, to monzodiorite, to monzonite near the northern contact with the Round Valley Peak Granodiorite. Lewis et al. (2021) provides detailed field descriptions, geochemistry, and geochronology from this complex.

Tamarack Lakes

The mafic body at Tamarack Lakes (2.3 km^2, 94.6 ± 1.1 Ma; this study) intruded into the quartz monzonite of Wheeler Crest (207 Ma; Stern et al., 1981) and is separated from the Hidden Lakes mafic complex by a 1.5-km-wide intrusion of the Lake Edison Granodiorite (93.5 Ma; Porter, 2013). Based on mapped geometries and coeval ages, it is possible that the Tamarack and Hidden Lakes bodies were once a single intrusion that was separated by subsequent Cretaceous intrusions. This body consists of mainly equigranular medium-grained amphibole-gabbro, which contains several ~100 m pods of diorite. The diorite can be either fine-grained and plagioclase dominated with small amphibole grains, or a coarse-grained network of acicular amphibole with interstitial plagioclase.

Pine Creek

The Pine Creek body (1.8 km^2) is made up of medium-grained amphibole-biotite gabbro through diorite with variable amounts of plagioclase. The mafic rocks were pervasively intruded by aplite dikes. Data from this study give the Pine Creek body an age of 194.0 ± 2.6 Ma, while Frost and Mattinson (1988) report an age of 97.5 ± 0.98 Ma via bulk zircon dissolution methods. Though we prefer a Jurassic age collected using a more modern analytical technique (laser ablation–inductively coupled plasma–mass spectrometry, LA-ICP-MS), it is possible

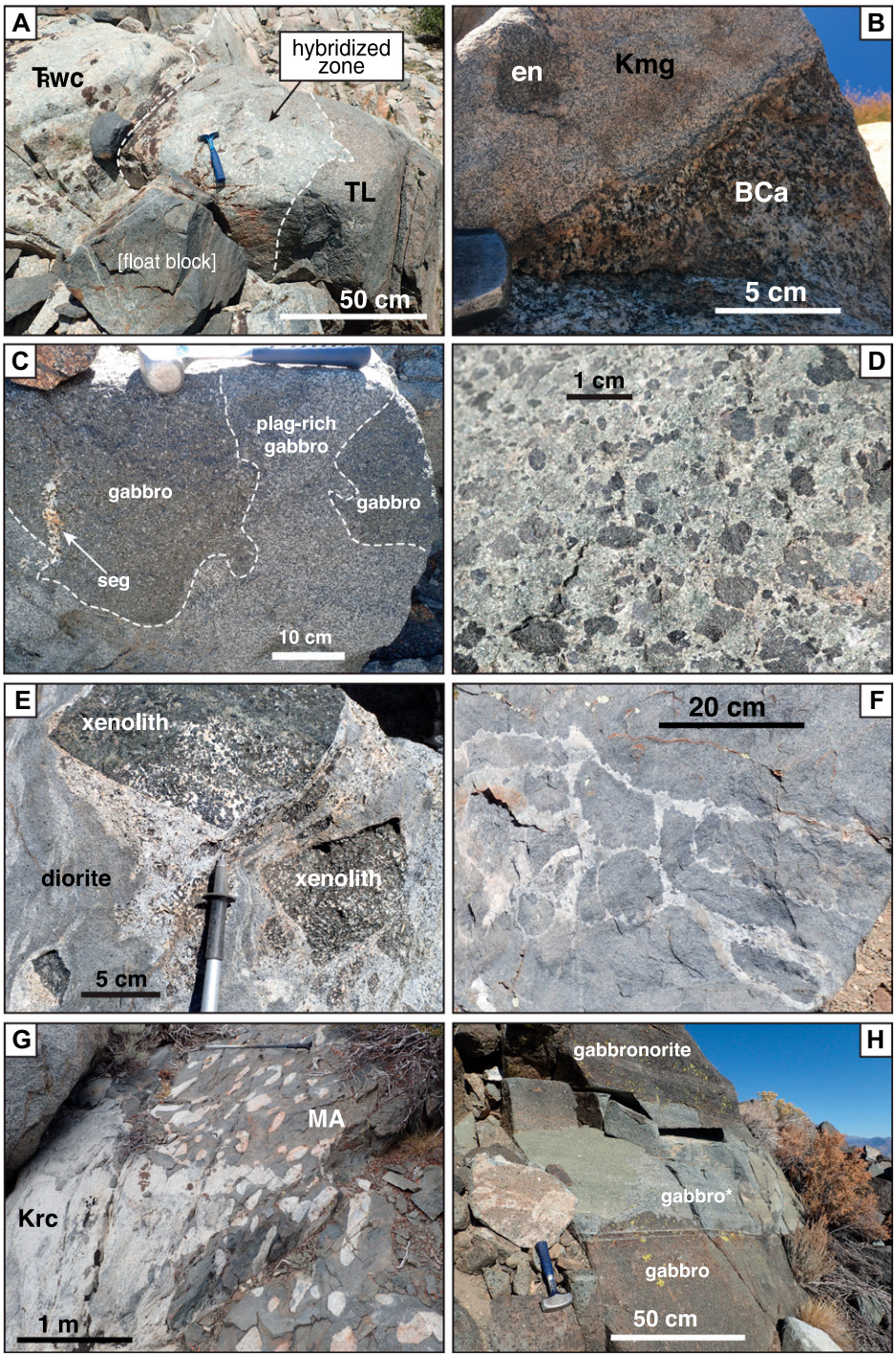

Figure 2. Field photos from the eastern Sierra Nevada batholith mafic complexes. (A) Gradational contact with a hybridized zone between the Wheeler Crest Quartz Monzonite (TRwc) and younger amphibole gabbro-diorite of Tamarack Lakes (TL). (B) Sharp contact where the McGann pluton (Kmg) intrudes the weakly foliated biotite-diorite of Black Canyon (BCa). Here, the McGann pluton contains a mafic enclave (en) that is unrelated to the Jurassic mafic complex. (C) Pods of cumulate gabbro surrounded by plagioclase-rich gabbro at Mount Tom. We interpret the plagioclase + amphibole segregation (seg) as late-stage melt extraction from the cumulates. (D) Porphyritic amphibole gabbro of McMurry Meadows. Black crystals are amphibole, and the fine-grained matrix is plagioclase and clinopyroxene. (E) Clinopyroxene-rich gabbro xenoliths in the Green Lake diorite, which is locally mingled with felsic septa. (F) Pillowed fine-grained diorite with felsic septa (lighter colored) in the Green Lake mafic complex. This diorite is an example of a texture that we consider melt-like. (G) Pipes of the leucogranite of Rawson Creek (Krc) where it intrudes the fine-grained gabbros of Mount Alice (MA). (H) Cumulate layering of gabbronorite (top) and gabbro (bottom) at McMurry Meadows. Note that the lightest colored area (labeled gabbro*) is part of the gabbroic layer, but it is light colored mainly due to recent exposure of the surface rather than a lithologic difference.

that the Pine Creek body is composite, containing both Jurassic and Cretaceous mafic intrusions that have not been distinguished by mapping. This complex is in contact with the granite of Chickenfoot Lake (191.8 ± 4.2 Ma; Lewis et al., 2021) on its northern side, which is coeval with our age for the Pine Creek diorite within uncertainty. The body is intruded by the Lake Edison Granodiorite (93.5 Ma; Porter, 2013) and Mono Creek Granite (87 Ma; Gaschnig, 2005).

Mount Tom

The Mount Tom Complex consists of one main body of amphibole-biotite gabbro and diorite (1.8 km^2) on the eastern flank of Mount Tom, surrounded by many smaller bodies that collectively cover ~1 km^2. This complex (145.1 ± 1.7 Ma; this study) intruded into the Tungsten Hills Quartz Monzonite (201.0 ± 2.6 Ma; this study) and the metasedimentary Permian-Pennsylvanian Pine Creek roof pendant. The gabbro and diorite of the Mount Tom Complex are marked by the occasional presence of very large biotite oikocrysts (up to 2 cm). Irregular pods of amphibole-gabbronorite cumulate 1–2 m in diameter are present within the gabbro (Fig. 2C). Many of the gabbro outcrops also contain plagioclase- and amphibole-rich lenses, which we interpret as products of segregated residual melts.

Tungsten Hills

The Tungsten Hills mafic body covers 1.3 km^2 on the eastern side of the Tungsten Hills near Bishop, California. The intrusion (148.3 ± 1.8 Ma; this study) was emplaced into the 202 Ma Tungsten Hills Quartz Monzonite (Stern et al., 1981). This body was also dated by Frost and Mattinson (1993) and Gevedon et al. (2021), with equivalent ages (within error) of 150.3 ± 1.5 Ma and 151.2 ± 0.7 Ma, respectively. The most common rock type is coarse-grained amphibole-biotite gabbro, with variably developed centimeter-scale layering. Few outcrops of plagioclase-rich amphibole-diorite

are found near the southern margin of the body. Garnet-bearing skarns and associated tungsten mines are common along contacts between gabbros and metasedimentary rocks (Bateman, 1965; Gevedon et al., 2021), though we avoided these areas when sampling.

Lake Sabrina

The mafic body at Lake Sabrina (91.1 ± 0.2 Ma; Coleman et al., 1995) is entirely diorite to quartz-diorite, with few associated basaltic dikes. The diorite covers an area of 4.3 km^2 and is generally medium to fine grained and contains both biotite and amphibole. Some diorite samples contain macroscopic titanite, up to 3 mm. This intrusion was co-magmatic with the neighboring Lamarck Granodiorite (91.9 ± 0.6 Ma; Coleman et al., 1995), as enclaves of the Lake Sabrina diorite were observed separating into and mingling with the Lamarck Granodiorite along the eastern margin of the diorite body (Frost and Mahood, 1987).

Bishop Creek

The mafic complex at Bishop Creek (146.5 ± 1.4 Ma) is located on the eastern side of South Fork Bishop Creek Canyon. The dominant rock type is biotite- and clinopyroxene-rich fine-grained gabbro (~2 mm grain size), which locally grades into coarser grained, porphyritic amphibole-gabbro (5–10 mm grain size). The northern margin of the complex consists of biotite-rich diorite. The mafic magmas intruded into the Tungsten Hills Quartz Monzonite, which was previously dated to 202 Ma in Pine Creek Canyon (Stern et al., 1981). Our new geochronology for the granitoid to the south of the mafic rocks, which is also mapped as the Tungsten Hills Quartz Monzonite, returns an age of 167.8 ± 1.6 Ma. Thin, elongate outcrops of metasedimentary rock are common within the complex, and multiple tungsten mining prospects within the complex exploited diopside, epidote, and garnet-bearing skarns that developed along contacts between metasedimentary and mafic units.

Green Lake

The mafic complex at Green Lake (97.1 ± 3.3 Ma; this study) consists of multiple hills and outcrops of amphibole-dominated diorite and gabbro, separated by extensive talus, which are potentially connected beneath the cover. We sampled the two largest mafic exposures, which sum to an area of ~1.1 km^2. Two main rock types are present: (1) porphyritic amphibole gabbro with coarse (1 cm) amphibole crystals surrounded by a matrix of fine-grained clinopyroxene and plagioclase (similar to Fig. 2D, though the photo is from McMurry Meadows), and (2) medium-grained amphibole-biotite gabbro that grades to diorite with increasing plagioclase content. Clinopyroxenite and gabbro xenoliths are also present within the diorite (Fig. 2E), which suggests that ultramafic cumulates are associated with this intrusion but are not exposed. Co-magmatic fine-grained diabase intrusions with pillow-like morphologies are present in the medium-grained gabbro and diorite (Fig. 2F), likely preserving melt compositions. The mafic rocks were intruded by the Lamarck Granodiorite (91.9 ± 0.6 Ma; Coleman et al., 1995) and the Inconsolable Granodiorite (95 Ma; Lackey et al., 2008) on the southern side of the complex.

Keough

The three bodies that make up the Keough Complex, located just west of Keough Hot Springs and covering an area of 0.85 km^2, intruded into the leucogranite of Rawson Creek (97.2 ± 1.1 Ma; this study; and 95 Ma; Stern et al., 1981) at 88.8 ± 1.3 Ma (this study). Lithologies are biotite-amphibole gabbro through diorite, with two internal bodies (~150–200 m) of coarse-grained, amphibole-rich cumulate with occasional clinopyroxene contained within amphibole cores. Metasedimentary xenolith blocks of up to 100 m in length were entrained within the gabbro; however, the origin of the blocks is unknown as the complex is not in contact with or near mapped metasedimentary rock units at the level of exposure.

Shannon Canyon

The Shannon Canyon mafic complex consists of six mapped mafic bodies summing up to 2.1 km^2. The lithologies are dominantly amphibole-diorite, with patches of foliated biotite-rich diorite (~50 m wide) and pods of diabase with amphibole and biotite phenocrysts in a fine-grained plagioclase-dominated matrix. The Shannon Canyon Complex (168.2 ± 1.9 Ma; this study) was contemporaneous, and possibly co-magmatic, with a granitoid mapped as the Tungsten Hills Quartz Monzonite, which produced an age of 170.8 ± 1.9 Ma at this location, though contacts are not well exposed for discernment of the intrusive relationships. The northern side of the complex was then intruded by a granite mapped as "rocks similar to the Cathedral Peak alaskite," abbreviated Kca (Bateman, 1965), with an age of 145.3 ± 1.2 Ma (this study).

Mount Alice

The Mount Alice mafic complex (146.1 ± 1.6 Ma; this study) is a series of small bodies exposed in both the south and north fork canyons of Big Pine Creek with a collective area of ~1 km^2. Originally, the complex likely comprised fewer larger intrusions, which were intruded and dissected by the leucogranite of Rawson Creek, dated locally to ca. 95 Ma by Stern et al. (1981). The mafic intrusions are in contact with the older Tinemaha Granodiorite (164 Ma; Bateman, 1992b) on the southern side of the complex. Angular fragments of fine-grained, biotite-bearing diabase and biotite-diorite, typically 5–10 cm in size, are common within the surrounding leucogranite of Rawson Creek, which suggests that portions of the Mount Alice Complex were brecciated by younger granitic intrusions. The complex contains two common lithologies: fine-grained amphibole-gabbro, and biotite-amphibole diorite. Enclaves of gabbro are contained within the diorite. In addition, coarse-grained, amphibole-rich cumulates crop out on the eastern side of Mount Alice. Leucogranite dikes and pods intruded the gabbro body at First Lake and mingled with the mafic lithologies, locally forming hybrid amphibole-diorite (<5 m wide areas). Rounded elongate pipes of the leucogranite, ~10–30 cm wide, intrude into the gabbros along the margins of the leucogranite pods (Fig. 2G).

McMurry Meadows

The McMurry Meadows Complex (also spelled MacMurray and McMurray in some publications) intruded into the Tinemaha Granodiorite (164 Ma; Bateman, 1992a) and the granodiorite of McMurry Meadows at 151.2 ± 1.7 Ma (this study). The McMurry Meadows mafic rocks were also dated by Frost and Mattinson (1993), who report an age of 150.8 ± 1.5 Ma. Sawka (1988) and Sawka et al. (1990) interpret the mafic complex and the granodiorite of McMurry Meadows as part of a bimodal, cogenetic fractionation sequence based on similarities between their trace element and Sr isotope signatures. The mafic complex consists of six main bodies, and the overall exposure of mafic rocks is roughly 2.4 km^2. The largest body is mainly composed of porphyritic amphibole gabbro, with amphibole crystals of up to 1 cm (~30%–40% modally), which can contain inclusions of clinopyroxene, olivine, and spinel. This gabbro is layered with gabbronorite cumulates (Fig. 2H) of a similar texture, though amphibole crystals are more common (up to 75% modally) and surrounded by a fine-grained orthopyroxene + clinopyroxene + plagioclase matrix (Fig. 2D). Near the intrusive margins with the granodiorite, the gabbro grades to porphyritic amphibole diorite.

Armstrong Canyon

We observe medium-grained amphibole- and biotite-bearing diorite and quartz-diorite within

the mafic complex at Armstrong Canyon (9.7 km^2), also referred to as the Aberdeen or Goodale Complex. Frost (1987) reports amphibole gabbro and layered biotite-amphibole gabbro at high elevations in the complex. Coleman et al. (1995) give a Late Cretaceous age for this complex of 91.5 ± 0.2 Ma, and they also date the coeval granite of Goodale Mountain (92.6 ± 1.2 Ma). Frost and Mattinson (1993) report a Jurassic age (153.8 ± 1.5 Ma) for this body. Mingling of the Armstrong diorite and granite of Goodale Mountain is exposed along the western margin of the complex (Coleman et al., 1995), which demonstrates that at least part of the complex is Cretaceous in age. The mafic body intrudes the Mule Lake pluton on its southwestern side, which gives an age of 158.4 ± 1.5 Ma (this study), as well as a Permian metasedimentary pendant.

Black Canyon

The Black Canyon mafic body (9.5 km^2, 157.2 ± 2.4 Ma; this study) intruded into the Mule Lake pluton (158.4 ± 1.5 Ma; this study) and Permian metasedimentary rocks. It was then intruded by the Spook pluton (103.8 ± 2.9 Ma; this study) on its northern side, the McDoogle pluton (94 Ma; Mahan et al., 2003) on the western side, and the undated McGann pluton to the south, which is inferred to be younger than the McDoogle pluton based on crosscutting intrusive relationships (Moore, 1963). As mapped, the northern portion of the complex is extensively cut by dikes, likely of the Independence dike swarm (148 Ma; Chen and Moore, 1979; Coleman et al., 2000), but the southern portion is not intruded by dikes while other nearby Jurassic plutons are pervasively intruded (such as the Tinemaha Granodiorite at Woods Lake, the Independence dike type locality). Thus, it is possible that the southern portion of the complex is younger than the northern side. Foliated, biotite-rich diorites (Fig. 2B) containing schlieren are common, and Frost (1987) reports mainly biotite gabbro from this body, as well as a pod of anorthosite in the high-elevation western section of the body.

Onion Valley

The mafic complex of Onion Valley (92.1 ± 0.3 Ma; Coleman et al., 1995) is the largest mafic intrusion in the eastern Sierra Nevada batholith (~25 km^2). The body consists predominantly of layered gabbros overlain by sheeted sills of basaltic through dioritic composition, with smaller layers of olivine-hornblendite. Detailed field description, compositional analyses, and crystallization modeling is presented in Sisson et al. (1996). The Onion Valley gabbro and sills intrude the Bullfrog pluton (103 Ma; Chen and Moore, 1982) to the south and the Dragon pluton to the north (103 Ma; Chen and Moore, 1982).

SAMPLING AND ANALYTICAL METHODS

Our sample suite includes 101 mafic samples from the 17 mafic intrusions described above, in addition to seven granitoid samples from previously undated plutons in the eastern Sierra Nevada batholith (Fig. 1B). Because there is significant textural and compositional variation within each body, we sampled the most representative rock type making up the majority of the exposed area, the most primitive lithology (typically cumulate rocks), the most evolved lithology (often diorites used for geochronology), and any fine-grained or pillow-like samples that could potentially represent frozen melts with liquid-like bulk compositions.

Bulk-Rock Geochemistry

Ninety-seven samples were analyzed for bulk-rock compositions via X-ray fluorescence spectrometry (XRF) at Caltech in Pasadena, California, USA (four samples were only collected for thin section). Samples for bulk-rock analysis were sawed to remove any potentially altered areas and sanded to remove saw marks or residue. To ensure homogeneity, ~0.5–1 kg of each sample rock was crushed and ~20 mL of crushed rock was powdered in an agate ball mill. Powders were dried overnight at 110 °C, then heated to 1050 °C for 1 hr to determine loss on ignition (LOI). Glass beads were prepared using a 10:1 mass ratio of Li-borate flux to sample powder and fused at 1200 °C. Major elements and a suite of trace elements (Si, Ti, Al, Fe, Mn, Mg, Ca, Na, K, P, Rb, Ba, Sr, Nb, Zr, Hf, Y, Zn, Cu, Ni, Co, Cr, V, La, Ce, Nd, Pb, and Th) in the glass beads were analyzed using a Panalytical Zetium wavelength-dispersive XRF spectrometer following the methods of Bucholz and Spencer (2019). Bulk-rock compositions and GPS locations of each sample are given in Table S3 (see footnote 1).

Olivine and Pyroxene Major Element Chemistry

Major element compositions of olivine, clinopyroxene, and orthopyroxene were analyzed in 28 samples using the JEOL JXA-8200 electron probe microanalyzer (EPMA) at Caltech. At least three points per grain were positioned to analyze both grain cores and rims to assess zoning, and at least five grains per sample were analyzed (where mineral abundances allowed) to ensure collection of representative mineral compositions. Elements analyzed were Si, Ti, Al, Cr, Fe, Mn, Mg, Ca, Na, K, and Ni. Detection limits were <0.006 wt% for Si, Al, Mg, Ca, and K; <0.02 wt% for Ti, Fe, Na, Cr, and Mn; and ~0.025 wt% for Ni. Operation conditions for the EPMA were a 25 nA beam current, a 15 kV acceleration voltage, and a focused beam diameter (<1 μm). For standardization, we used synthetic forsterite, fayalite, Mn-olivine, anorthite, TiO_2, NiO, and Cr_2O_3, and natural standards Amelia albite and Asbestos microcline. We used a mean atomic number (MAN) background correction and the CITZAF matrix correction program (Armstrong, 1995) for data reduction.

Zircon U-Pb Geochronology

We separated zircon from 20 samples, including 13 gabbros and diorites and seven granitoids, and mounted between 25 and 52 grains per sample. Zircon grains were polished and imaged for cathodoluminescence response on the Zeiss 1550 VP field emission scanning electron microscope at Caltech. U-Pb isotopic data in zircon were measured via LA-ICP-MS at the Arizona Laserchron Center, Tucson, Arizona, USA, following the methods of Pullen et al. (2018). Zircon were analyzed using a Photon Machines 193 nm G2 excimer laser attached to a Thermo Scientific™ Element 2™ high-resolution single collector ICP-MS. Laser conditions were a 30 μm spot diameter, 7 Hz frequency, 7 J/cm^2 fluence, and 380 shots per analysis. Masses analyzed were ^{202}Hg, $^{204}(Hg + Pb)$, ^{206}Pb, ^{207}Pb, ^{208}Pb, ^{232}Th, and ^{235}U. Analytical dwell times for each mass ranged from 0.001 s to 0.3 s. Laser spots were placed near grain rims. Primary standards Forest Center gabbroic anorthosite (FC, Paces and Miller, 1993) and Sri Lanka zircon (SL, Gehrels et al., 2008) were placed between every five unknown analyses and used to correct for drift in the ICP-MS and down-hole fractionation. A secondary standard, R33 (Mattinson, 2010), was measured between every 20 and 30 analyses.

Data were reduced using the Excel-based reduction program AgeCalc (Gehrels et al., 2008). Crystallization ages were calculated in IsoplotR (Vermeesch, 2018) as an error-weighted mean of individual spot $^{206}Pb/^{238}U$ ages for each sample, and reported uncertainties are propagated errors from all single-grain analyses included in the mean age (2σ). Analyses identified as discordant by AgeCalc filters or as outliers by the IsoplotR Chauvenet's criterion (Gehrels et al., 2008; Vermeesch, 2018) were excluded from the weighted mean age calculation, resulting in 11–40 acceptable analyses per sample.

RESULTS

Geochronology

New geochronological results from 13 mafic bodies (Table 1) and seven previously undated granitoid plutons (Table 2) in the eastern Sierra Nevada batholith are shown in Figure 3, along with the ages of six previously dated mafic intrusions and granitoids associated with each mafic body. Representative cathodoluminescence (CL) images of grains dated are shown in Figure S3 (see footnote 1), and weighted mean age and concordia plots for each newly dated sample are shown in Figure S4 (see footnote 1). A summary of new geochronology is given in Table S1, and U-Pb isotopic measurements for each zircon grain are given in Table S2 (see footnote 1).

Grains identified as outliers significantly older than the weighted mean age were interpreted to be grains inherited from either older parts of the batholith or from metasedimentary and metavolcanic wall rocks. These grains are uncommon (~3% of analyses, with a maximum of five per sample), which indicates minimal retention of preexisting zircon in the mafic magmas, and thus little effect on the measured ages. An exception is the dated diorite from Cargyle Meadows, wherein nearly one-third of the concordant analyses (5/16 grains) returned ages >10 m.y. older than the dominant age population. These grains were excluded from the reported weighted mean age and were likely inherited from unexposed sources located at a deeper level in the batholith. Inheritance is also a likely source of anomalously old grains from

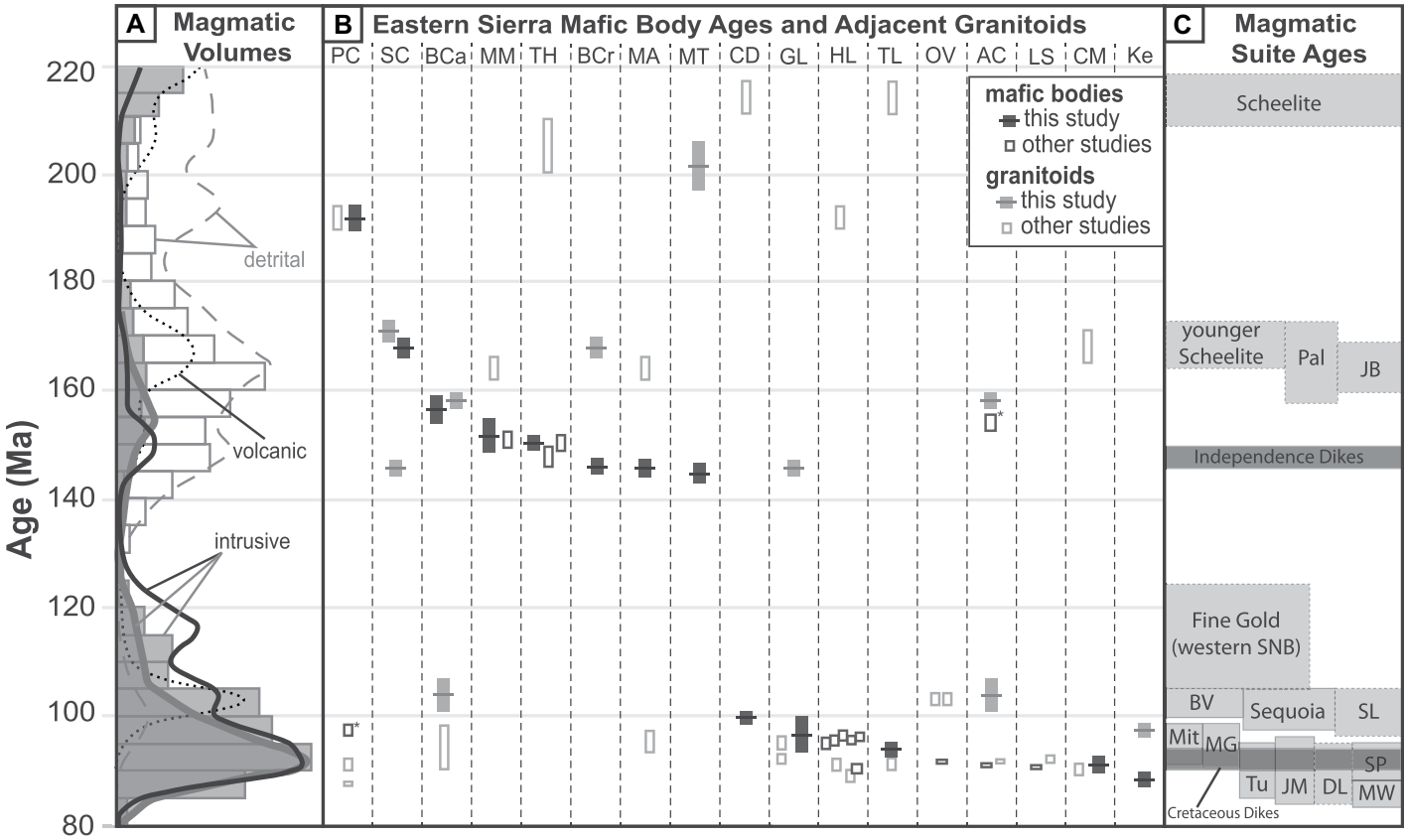

Figure 3. Summary of geochronology in the eastern Sierra Nevada batholith (SNB) relevant to the mafic bodies in this study. (A) Areal extent of granitoids and zircon abundance over time in the Sierra Nevada batholith, commonly interpreted as correlated with volumetric magmatic flux. Volcanic (dotted), intrusive (solid black), and detrital (dashed) curves are from Attia et al. (2020). The thick gray curve is intrusive flux from Ducea (2001), and intrusive (gray filled) and detrital (white) bars are from Paterson and Ducea (2015). Curves are normalized to display equivalent intensities during the Late Cretaceous peak (ca. 92 Ma). (B) Geochronological data from the central-eastern Sierra Nevada batholith. New ages are shown as filled bars, and previously published ages (see Table 1 for references) are plotted as open bars. Abbreviations are as in Figure 1. Granitoids plotted in the same column as a mafic body are in contact with that mafic intrusion. Note that new granitoid ages from the Spook pluton (103.8 ± 2.9 Ma), Mule Lake pluton (158.1 ± 1.3 Ma), and Kca ("rocks similar to the Cathedral Peak alaskite"; Bateman, 1965) (145.6 ± 1.3 Ma) are each plotted twice, as both are adjacent to two of the mafic bodies in this study. *Two preexisting ages in panel B (PC and AC; Frost and Mattinson, 1993) do not agree with more recently collected data. These mafic bodies could be composite, containing both Jurassic and Cretaceous intrusions, or these data (from analysis of U-Pb in bulk zircon separates) may be erroneous. (C) Age ranges of major magmatic suites and dike swarms in the Sierra Nevada batholith. Solid outlines indicate nested suites, while dashed outlines represent non-nested suites. Age references are as follows: Scheelite (Barth et al., 2011), Palisade Crest (Pal) and Shaver Lake (SL) (Bateman, 1992a), Jawbone (JB) (Stern et al., 1981), Sonora Pass (SP) (Leopold, 2016), Bear Valley (BV) (Klein and Jagoutz, 2021), Sequoia (Lackey et al., 2008), Mitchell (Mit) (Chen and Moore, 1982; Sisson and Moore, 2013), John Muir (JM) (Davis et al., 2012), Mount Givens (MG) (Frazer et al., 2014), Domelands (DL) (Saleeby et al., 2008), Fine Gold (Lackey et al., 2012), Tuolumne (Tu) (Coleman et al., 2004), Mount Whitney (MW) (Hirt, 2007), and Independence and Cretaceous dikes (Coleman et al., 2000).

Keough (n = 3), Casa Diablo (n = 2), Tungsten Hills (n = 1), Shannon Canyon (n = 1), and the leucogranite of Rawson Creek (n = 2). The vast majority of grains analyzed are concordant (Figure S4), with only 6% of analyses excluded for discordance. CL images (Fig. S3) do not show resorbed cores or clearly separate age domains within individual grains. Zircon grains from the gabbros and diorites display sector zoning or oscillatory zoning or lack clear zoning (Fig. S3). Most zircon grains from the granitoids show concentric oscillatory zoning. Some inherited grains display complex internal textures that likely result from recrystallization after assimilation. Thus, the measured age of inherited grains may not accurately represent the crystallization age of the rock from which the grain was inherited.

The 13 mafic bodies dated in this study and previously dated mafic intrusions (Coleman et al., 1995; Lewis et al., 2021) in the eastern-central Sierra Nevada batholith that were not dated here reveal two major episodes of mafic magmatism from 168 Ma to 145 Ma (n = 7) and 100 Ma to 89 Ma (n = 9) in this study area. The Pine Creek intrusion is an outlier, as it crystallized in the Early Jurassic at 192.3 ± 2.4 Ma (Table 1, Fig. 3). The Shannon Canyon intrusion represents the oldest intrusion of the main Jurassic episode, having crystallized at 168.3 ± 1.8 Ma. The youngest dated Jurassic mafic body is the Mount Tom intrusion at 145.1 ± 1.7 Ma. The Cretaceous episode is bracketed by the Casa Diablo intrusion (100.2 ± 1.1 Ma) and the Keough intrusion (88.8 ± 1.3 Ma). Many of the mafic bodies are in contact with at least one granitoid pluton that is broadly coeval with the mafic intrusion within age uncertainties (n = 9/17; Fig. 3). The episodes of mafic magmatism spatially and temporally overlap with voluminous granitoid intrusions in the Sierra Nevada batholith, including younger portions of the Scheelite intrusive suite (Bateman, 1992a), the Palisade Crest intrusive suite in the Late Jurassic (Stern et al., 1981; Bateman, 1992a), and the John Muir and Mount Givens intrusive suites in the Late Cretaceous (Frazer et al., 2014; Davis et al., 2012). Concomitant and co-located mafic and felsic magmatic activity indicates a close connection between the production of mantle melts and intrusion of voluminous felsic plutons and allows for a cogenetic link between mafic and felsic plutons within intrusive suites in the Sierra Nevada batholith.

Mineral Occurrences and Major Element Chemistry

To assess the degree of differentiation of the melts parental to the mafic complexes, we analyzed major element compositions of olivine, clinopyroxene, and orthopyroxene (Table S5; see footnote 1). Amphibole and biotite are dominant in these complexes, but crystallized later, at lower Mg#, than olivine or pyroxenes, so we targeted the early crystallizing phases for calculations of initial melt compositions. We report mineral compositions from 11 of the 17 mafic bodies in this study (Fig. 4), as olivine and/or pyroxenes were not found in our samples from the Tamarack Lakes, Armstrong Canyon, Shannon Canyon, Black Canyon, and Lake Sabrina bodies. Thin-section images are shown in Figure S2. Mineral data from the Hidden Lakes and Onion Valley complexes are presented in Lewis et al. (2021) and Sisson et al. (1996), respectively.

Within the eastern Sierra Nevada batholith mafic bodies in this study, olivine was found only at the Hidden Lakes (Lewis et al., 2021), McMurry Meadows, Onion Valley, and Casa Diablo bodies. The most primitive unaltered olivine grains in each intrusion have Mg#s ranging from 77 to 82, and the full range of olivine compositions we analyzed span Mg#s 71–87, wherein all grains with Mg# > 82 exhibit subsolidus Fe-Mg exchange with Fi-Ti oxides.

Orthopyroxene is present in gabbro and gabbronorite in five of the 11 mafic bodies that we analyzed for mineral chemistry (Bishop Creek, Keough, Mount Tom, Casa Diablo, and McMurry Meadows), and is a major phase in norite cumulates in parts of the Hidden Lakes body (Lewis et al., 2021). Mg#s in measured orthopyroxene range from 46 to 77. Intercumulus orthopyroxene is reported in the Onion Valley Complex (Sisson et al., 1996).

Clinopyroxene is present in our samples from the majority of mafic bodies in this study, except for the Tamarack Lakes, Armstrong Canyon, Shannon Canyon, Black Canyon, and Lake Sabrina bodies. Some clinopyroxene has experienced metamorphic Tschermak exchange ($[Fe, Mg]_2Si_{-1}Al_{-1}$) during cooling, and the following describes populations of clinopyroxene with chemistries that represent the least such exchange (high Al compared to Mg atoms per formula unit). Typical clinopyroxene in samples from Keough, Hidden Lakes, Casa Diablo, Mount Tom, and Bishop Creek are 1–2 mm subequant, subhedral to somewhat anhedral, and rimmed by amphibole. Frequently, there is patchy reaction to amphibole within the crystal, and some grains have very thin exsolution lamellae. These grains range in Mg# from 71 to 80. At Bishop Creek, this range extends lower (to Mg# 61), and clinopyroxene in samples associated with skarn mineralization extends as high as Mg# 82. However, we do not include mineralized skarn samples in our discussion, as they may have been affected by exchange with metamorphic roof pendant blocks in the body. Clinopyroxene in samples from Cargyle, Mount Alice, Tungsten Hills, and Pine Creek are smaller (0.25–0.5 mm), and found as anhedral-reacted cores within amphibole, with Mg#s ranging from ~65 to 79; these have lower Al atoms per formula unit than the larger grains described above and may have experienced metamorphic exchange, but they overlap with the range of Mg# of the large grains and thus are included in parental melt calculations (see below). Clino-

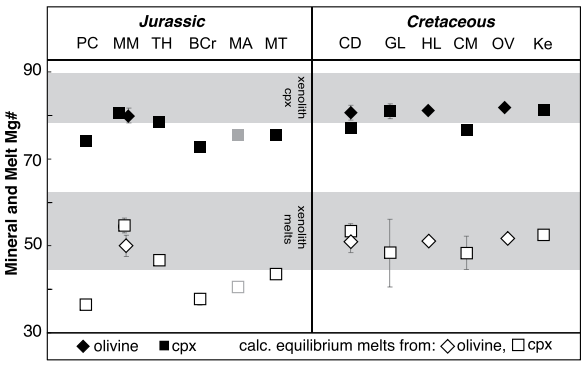

Figure 4. Magnesium numbers (Mg# = Mg/[Mg + Fe^T]) of ultramafic minerals and equilibrium melt compositions calculated. For each body containing olivine and/or clinopyroxene (cpx), we plot a mineral Mg# as the average of the most primitive population of mineral grains from each complex (n = 1–10 analyses, solid symbols) and 2σ uncertainties. Abbreviations are as in Figure 1. Only one acceptable clinopyroxene analysis was collected from Mount Alice (MA) samples, which are indicated by the gray symbols. Mineral data for Hidden Lakes (HL) are from Lewis et al. (2021), and Onion Valley (OV) data are from Sisson et al. (1996). Equilibrium melt compositions were calculated using the most primitive mineral populations from each mafic body; see text for further discussion (open symbols and 2σ uncertainties). Shaded areas denote the range of Mg#s for clinopyroxenes and calculated equilibrium melts for low-MgO cumulate xenoliths thought to originate from the lower crust of the Sierra Nevada batholith (Lee et al., 2006). Calculation of equilibrium melts for xenoliths was done in the same manner as for the mafic bodies.

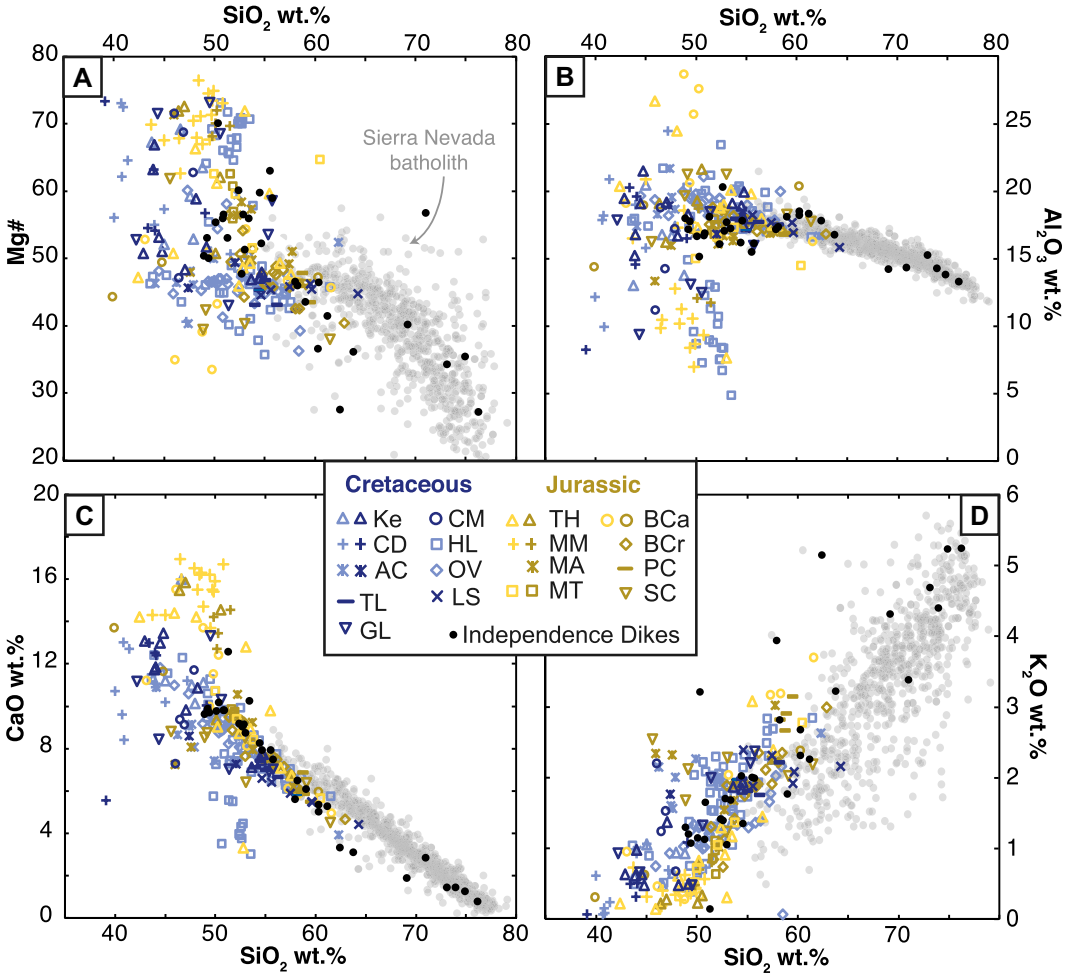

Figure 5. Bulk-rock compositions for mafic bodies in the area studied, including analyses from this study, Hidden Lakes (HL; Lewis et al., 2021), Onion Valley (OV; Sisson et al., 1996), and Frost (1987). SiO_2 versus (A) Mg#, (B) Al_2O_3, (C) CaO, and (D) K_2O. Jurassic samples are shown in yellow and Cretaceous samples are in blue, and samples new to this study are shown in darker shades. Compositions of dikes from the Independence dike swarm are from Glazner et al. (2008). Sierra Nevada batholith plutonic compositions are from the GEOROC database and filtered for oxide totals between 98 wt% and 102 wt%. Abbreviations are as in Figure 1.

pyroxene from porphyritic amphibole gabbro at both Green Lake and McMurry Meadows has two distinct populations that overlap in Mg#. One higher Al population with Mg# of 77–82 is typically 0.25–0.5 mm, euhedral to anhedral crystals, and frequently poikilitically enclosed by large amphibole oikocrysts (Fig. S2). A second low Al population with Mg# of 76–81 is found as smaller light-green grains that are euhedral to subhedral or frequently rounded in clusters surrounded by late-crystallizing interstitial plagioclase, and it is not included in amphibole.

Bulk-Rock Major and Trace Element Chemistry

Bulk-rock compositions in our sample suite range from 39.1 wt% SiO_2 to 64.3 wt% SiO_2 and have Mg#s of 38–74. SiO_2 contents within each body vary by at least 10 wt% for the majority of plutons and overlap with intermediate plutons (diorites, tonalites, and granodiorites) in the Sierra Nevada batholith. Oxide versus SiO_2 variation diagrams for the mafic bodies form trends continuous with the range of Sierra Nevada batholith granitoid bulk compositions (from the GEOROC database, georoc.eu; Figs. 5 and S5; see footnote 1). There is more compositional scatter in mafic bodies than in the felsic portion of the Sierra Nevada batholith, likely reflecting a greater range from melt-like to cumulate-dominated lithologies in the mafic intrusions than in the granitoids.

Concentrations of CaO, FeO, MnO, and TiO_2 linearly decrease from the lowest SiO_2 cumulates through high-silica granites (79 wt% SiO_2). Likewise, K_2O content increases linearly with increasing SiO_2 content. Between SiO_2 contents of 38–55 wt%, Al_2O_3 content ranges from 4.9 wt% to 28.7 wt% and is not strongly correlated with SiO_2. The low Al_2O_3 (<17 wt%) samples are pyroxene- and amphibole-dominated cumulates with little plagioclase, while the high Al_2O_3 (>20 wt%) samples in this silica range likely accumulated plagioclase. At SiO_2 contents greater than 55 wt%, Al_2O_3 decreases with increasing SiO_2 and is contiguous with the Sierra Nevada batholith granitoid trend. This is very similar to the variation in Sr content (Fig. S5), which is highly variable (20–1370 ppm) at low SiO_2 contents, and then decreases continuously with the rest of the batholith in samples with >55 wt% SiO_2, further supporting a plagioclase control on this trend. Variations in Al_2O_3 and Sr contents are also consistent with Na_2O evolution, which has a wide range of concentrations (0.03–4.5 wt%) in samples with SiO_2 contents of between 38 wt% and 55 wt% and increases rapidly with SiO_2 content in this range. In more evolved samples (>55 wt% SiO_2), Na_2O content remains steady at an average of 3.6 wt%, which is consistent with the bulk of the Sierra Nevada batholith. MgO content and Mg# also vary broadly in samples with less than 55 wt% SiO_2, from 1 wt% to 20 wt% and 34–76, respectively. As SiO_2 increases, MgO and Mg# follow decreasing trends that adjoin to the range of Sierra Nevada batholith granitoids (Fig. 5A). The rapid decrease in MgO (and thus Mg#) at low SiO_2 contents is likely a factor of olivine, clinopyroxene and orthopyroxene, and amphibole fractionation, which generates mafic cumulates with variable amounts of plagioclase.

DISCUSSION

Parental Melt Compositions of Mafic Bodies and Differentiation Histories

One goal of this study is to quantify the composition of the parental melts of the mafic complexes. We define "parental melt" as the most primitive (i.e., highest Mg) melt to intrude into each mafic complex at the level of emplacement. Based on the prevalence of amphibole gabbro to gabbronorite-dominated cumulates in many of the mafic complexes sampled (as indicated by textures and trace element composition indicative of the accumulation of plagioclase), it is likely that this melt differentiated within the upper crust to produce cumulates and more evolved liquids. Thus, we cannot directly sample and analyze the parental melt composition with certainty. Instead, we use the compositions of the most primitive olivine, clinopyroxene, and orthopyroxene grains found in cumulates in each mafic complex to calculate the Mg# of a melt in equilibrium with these phases. We do not use amphibole to calculate equilibrium melt compositions as Fe^{2+}/Mg mineral-melt distribution coefficients for amphibole are not well determined, and relative abundances of ferric and ferrous iron are difficult to accurately constrain in amphibole using EPMA analyses.

First, we selected only the mineral analyses that best represent primary magmatic compositions unaltered by secondary, subsolidus processes. For example, olivine grains exhibiting Fe-Mg exchange with Fe-Ti-oxides were excluded, as their exceptionally high Mg#s (Mg# 82–87) result from Fe removal. For clinopyroxene, analyses with low Al atoms per formula unit (APFU) were filtered out at thresholds depending on the mafic body, to exclude analyses affected by subsolidus Tschermak exchange (Al APFU thresholds: 0.15 for Keough, Cargyle, and Green Lake; 0.10 for Mount Tom; 0.16 for McMurry Meadows; 0.06 for Tungsten Hills; 0.117 for Bishop Creek). The populations of clinopyroxene with the highest Mg# analyses remaining after applying the Al filter were then selected as representative of the most primitive primary magmatic clinopyroxene compositions. The Mount Alice and Pine Creek bodies had very few clinopyroxene grains and analyses (1 and 6, respectively) and do not vary in Al atoms per formula unit, so we used the highest Mg# population.

After these considerations, the following experimentally determined Fe^{2+}/Mg mineral-melt distribution coefficients were used for this calculation: 0.303 for olivine, 0.284 for orthopyroxene (Beattie, 1993), and 0.23 for clinopyroxene (Sisson and Grove, 1993). In olivine, we assume all iron is Fe^{2+}. In clinopyroxene and orthopyroxene, we calculated atoms per formula unit (APFU, Table S5) of ferric and ferrous iron, using only the ferrous iron in the equilibrium melt calculation. We utilized a ferric iron to total iron ratio of 0.18 in the melts, consistent with an oxygen fugacity (fO_2) at the nickel-nickel oxide buffer as determined using the MELTS supplemental calculator at a temperature of 1150 °C (Ghiorso and Sack, 1995), which is a typical fO_2 for continental arc magmas and in agreement with those calculated for the Hidden Lakes mafic complex (Lewis et al., 2021). Mineral compositions from the most primitive grains in each body, as well as the calculated parental melt Mg#s, are included in Table S4 (see footnote 1).

For bodies containing a combination of olivine, clinopyroxene, and/or orthopyroxene, we took the highest Mg# calculated melt to be the parental melt composition. Figure 4 shows only olivine and clinopyroxene analyses, because clinopyroxene returned melt Mg#s that are 2%–20% higher than melts calculated based on orthopyroxene. In the Shannon Canyon, Lake Sabrina, Tamarack Lakes, Armstrong Canyon, and Black Canyon complexes, we did not observe olivine or pyroxenes (there were only amphibole and/or biotite at those localities), so a parental melt composition based on well-established partition coefficients could not be calculated.

Calculated parental melts have Mg#s ranging from 37 to 55 (Fig. 4), which represent the parental melt to each mafic body prior to substantial upper crustal differentiation. These reported parental melt Mg#s are minimum estimates, as we have not sampled or analyzed every mineral within each complex. However, two mafic bodies have been studied in great detail, the Onion Valley (Sisson et al., 1996) and the Hidden Lakes complexes (Lewis et al., 2021), and they support our inference that the highest Mg# mineral analyzed from these localities (unmodified by secondary processes) likely crystallized from a parental melt composition. The parental melt Mg# calculated for these two localities is 51–52. The calculated parental melts in the majority of the mafic bodies (8 of 12) are within 50 ± 5, with the others being slightly more evolved and lower in Mg#.

The mafic melts that intruded into the upper crust of the eastern Sierra Nevada batholith to form these mafic bodies were not consistent with primitive melts of the mantle (Mg# = ~65–70) and must be the products of the differentiation of high-MgO melts. Differentiation from high-MgO melts likely occurred at depth prior to ascent to the upper crust. Thus, the melts that are parental to the suite of mafic bodies experienced both lower crustal and later upper crustal differentiation, as supported by models of polybaric fractionation in the Sierra Nevada batholith (Sisson et al., 1996; Lewis et al., 2021) and in other arc batholiths (Almeev et al., 2013; Hamada et al., 2014; Melekhova et al., 2015; Marxer et al., 2022). Evidence of high-pressure differentiation processes within the Sierra Nevada batholith can be found in the lower crustal Bear Valley intrusive suite and as mafic to ultramafic cumulate xenoliths thought to originate from deep portions of the Sierra Nevada batholith crust. The Bear Valley intrusive suite, exposed in the southernmost and most deeply exhumed section of the Sierra Nevada batholith, contains norite and hornblende-gabbro cumulates that crystallized between 0.7 GPa and 0.9 GPa (Pickett and Saleeby, 1993; Klein and Jagoutz, 2021; Rezeau et al., 2021). The Bear Valley intrusive suite lithologies are similar to the most primitive cumulates found in the 100–300 MPa (Ague and Brimhall, 1988) upper crustal mafic bodies in this study. Maximum bulk-rock Mg#s of Bear Valley intrusive suite gabbros (~73) are roughly equivalent to bulk-rock Mg#s from the McMurry Meadows (~76), Hidden Lakes (~74), and Casa Diablo (~73) mafic bodies (Klein and Jagoutz, 2021; Lewis et al., 2021). The production of similar cumulate compositions at different depths in the Sierra Nevada batholith indicates that fractionation of mafic magmas occurred in both the upper and lower crust and suggests that the parental melts to the upper crustal mafic bodies and to the Bear Valley intrusive suite gabbroids were similarly evolved non-primitive basalts. Cretaceous high-pressure (2–3 GPa) garnet-pyroxenite cumulate xenoliths from the Sierra Nevada batholith (Dodge et al., 1986, 1988; Mukhopadhyay and Manton, 1994; Lee et al., 2001, 2006) could be the cumulate counterparts of the low-Mg basalts parental to the upper crustal mafic bodies, as previously suggested (e.g., Lee et al., 2006). Clinopyroxene from the lowest MgO pyroxenes in these xenoliths would be in equilibrium with melt compositions in the same Mg# range as the parental melts to all of the Cretaceous, and many of the Jurassic, mafic bodies (Fig. 4).

As the mafic complexes studied here contain abundant amphibole and biotite, they originate from hydrous, relatively low-density melts that are able to ascend buoyantly through the arc crust. For example, melts parental to the Onion Valley Complex (Mg# = 60, 4–6 wt% H_2O) have densities of 2.45–2.55 g/cm^3, which would be buoyant in the surrounding granitoid crust (2.60–2.69 g/cm^3; Sisson et al., 1996). Additionally, the parental melt to the Hidden Lakes mafic complex (Mg# = 51, 3.1 wt% H_2O; Lewis et al., 2021) has a calculated density of 2.51 g/cm^3. This supports the inference that evolved basalts

are buoyant enough to ascend after sufficient lower-crustal fractionation.

Crustal Thickness Estimates from the Eastern Sierra Nevada Batholith

Bulk-rock Sr/Y ratios (Fig. 6A) have been used as a proxy for crustal thickness or depth to the Moho in arcs, relying on the pressure dependence of plagioclase and garnet stability during fractionation and partial melting (Chapman et al., 2015; Profeta et al., 2015). At depths where plagioclase is stable (<1 GPa), Sr is incorporated into plagioclase-bearing cumulates or partial melt residues, which results in lower Sr/Y ratios in equilibrium melts. At higher pressures in the absence of plagioclase, Sr is relatively incompatible in the cumulate or residue assemblage, but Y strongly partitions into residual and fractionating garnet, which leads to higher Sr/Y ratios in melts generated at these depths. Based on these predictions, Profeta et al. (2015) developed a crustal thickness proxy based on a global database of intermediate (55–68 wt% SiO_2) volcanic rocks from arcs displaying a positive linear correlation between bulk-rock Sr/Y and Moho depths. This method was designed to be applied on non-primitive, intermediate compositions and thus to yield information on the depth of crustal differentiation. However, Sr/Y ratios in arc magmas could more appropriately be viewed as a proxy for understanding the depth of the most recent stage of magma differentiation, whether that is the segregation of mantle melts from a residue or crystallization within the crust. For example, the thermal structure of the mantle wedge, and thus the depth and extent of melting, is controlled by lithospheric thickness (Turner et al., 2016), and would lead to the same effect in Sr/Y. Deeper, lower extents of mantle melting in the garnet stability field due to thicker arc crust would lead to higher Sr/Y in primitive melts, and thinner crust would lower Sr/Y due to increased melting at shallower pressures where garnet is not stable.

However, when applying this proxy for crustal thickness, some complications may arise. For example, the Sr budget of primitive arc magmas is also strongly influenced by contributions from the subducting slab, which is independent of the pressure of differentiation (Sisson and Kelemen, 2018; Turner and Langmuir, 2022). Furthermore, crystallization of amphibole, which is stable over a range of crustal pressures, would increase Sr/Y in melts as it preferentially incorporates Y over Sr (Nandedkar et al., 2014). If differentiation involves both amphibole and plagioclase, then melt Sr/Y may increase, decrease, or be invariant depending on the relative proportion of the differentiating phases. Finally, earlier stages of differentiation may be overprinted by assimilation, and/or by later, shallower fractionation.

With these caveats in mind, we proceed cautiously in calculating crustal thicknesses at the time of intrusion for the Sierra Nevada batholith mafic bodies using the Profeta et al. (2015) calibration. Although the Profeta et al. (2015) crustal thickness model is calibrated for intermediate volcanic bulk compositions (55–68 wt% SiO_2), the Sr/Y values for mafic Sierra Nevada batholith samples (Sr/Y average = 35, SiO_2 = 45–55) are roughly equivalent to intermediate Sierra Nevada batholith samples (Sr/Y average = 33) within admittedly considerable scatter (Fig. S6; see footnote 1), and thus are likely still faithful recorders of crustal thickness despite falling outside of the calibrated compositional range. One potential reason for this broad similarity is that differentiation to produce more felsic melts from mafic compositions involves both plagioclase and amphibole crystallization, which limits variations in Sr/Y during melt evolution.

When applying this proxy to the plutonic record, it is important to make an extra effort to apply this only to samples that are thought to be melt-like. As there is evidence for differentiation within the Sierra Nevada batholith mafic bodies, as discussed above, we only use samples that display non-cumulative textures (dikes or fine-grained), with bulk-rock Sr/Nd and Al/Si values that suggest negligible plagioclase or amphibole accumulation (Fig. S7; see footnote 1). To minimize the effects of upper crustal fractionation on Sr/Y ratios, we also only used samples with Mg#s within the range of the calculated parental melts. Indeed, our mafic samples (SiO_2 < 55 wt%), with textures and compositions suggesting that they are melt-like, define a narrower range of Sr/Y values (Sr/Y = 21–57) than do either the full suite of mafic samples (SiO_2 < 55 wt%, Sr/Y = 4–106) or the entire population of Sierra Nevada batholith intermediate samples included in the NAVDAT database (SiO_2 = 55–68 wt%, Sr/Y = 7–100; Fig. S6). The more limited variation in the melt-like mafic samples likely results from a decrease in noise related to plagioclase and amphibole accumulation/fractionation affecting the cumulate mafic and more felsic lithologies from the Sierra Nevada batholith. In rocks with >68 wt% SiO_2, minimum Sr/Y decreases with increasing SiO_2 content, likely reflecting the depletion of Sr in the remaining melt due to extensive plagioclase crystallization.

Using the subset of melt-like samples (identified in Table S3), we calculated an average crustal thickness of 32–38 km for the Middle–Late Jurassic mafic bodies and 40–51 km (average 44 km) for the Cretaceous mafic bodies. The youngest Cretaceous (<95 Ma) samples (e.g., Keough, 88.8 Ma and 51 km) record the

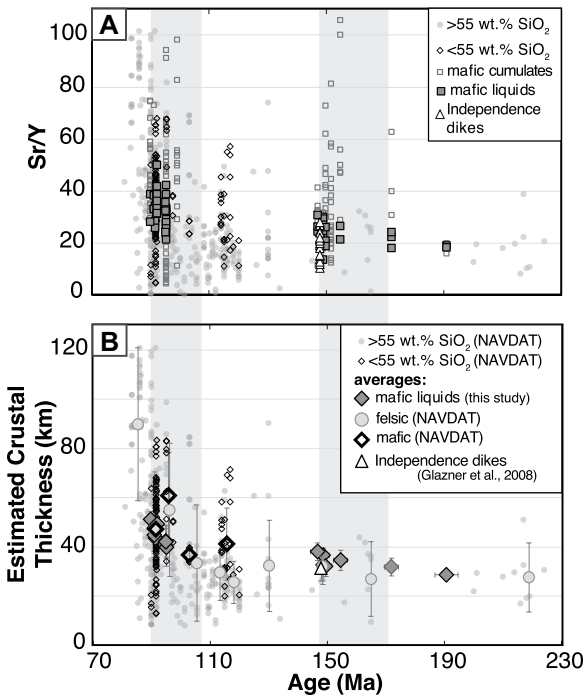

Figure 6. Trace element ratios and estimated crustal thickness in the Sierra Nevada batholith (SNB) over time. Vertical gray bars indicate periods of enhanced magmatism in the Sierra Nevada batholith associated with the building of intrusive suites. (A) Bulk-rock Sr/Y ratios in individual mafic and felsic samples in the Sierra Nevada batholith. Samples >55 wt% and <55 wt% SiO_2 are from Lackey et al. (2008) and the North American Volcanic and Intrusive Rock Database (NAVDAT; http://www.navdat.org). Compositions of dikes from the Independence dike swarm are from Glazner et al. (2008). Mafic cumulates and liquid-like samples are from this study and Frost (1987). (B) Crustal thicknesses calculated from bulk-rock Sr/Y ratios (Profeta et al., 2015). Average compositions not from this study are taken from the NAVDAT database and Lackey et al. (2008). Error bars are 1σ of all crustal thicknesses calculated from melt-like samples, per mafic body.

thickest crust (Fig. 6B). Shallower depths were recorded by the Early Jurassic Pine Creek body (29 km). Crustal thicknesses calculated from dikes in the 148 Ma Independence dike swarm (Chen and Moore, 1979; Glazner et al., 2008) are 32 ± 3 km for mafic dikes (<55 wt% SiO_2) and 27 ± 6 km for intermediate and felsic dikes (>55 wt% SiO_2), in broad agreement with estimates from the Jurassic mafic bodies of the eastern Sierra Nevada batholith (Fig. 6B). The maximum crustal thicknesses calculated from granitoids increase consistently with the mafic liquid-like samples. However, Sr/Y ratios recorded by mafic liquids and calculated crustal thicknesses display a narrower range of values than we calculated for contemporaneous granitoids (Fig. 6), which supports our assertion that mafic melt-like samples are ideal for crustal thickness calculations using bulk-rock Sr/Y. Our thickness calculations are in broad agreement with crystallization depth estimates from Cretaceous Sierran garnet-pyroxenite cumulate xenoliths, which originated at a minimum of 45 km depth (Lee et al., 2001).

Relationship between Mafic and Felsic Magmatism in the Sierra Nevada Batholith

Although two distinct periods of magmatism in the Late Jurassic and Late Cretaceous (commonly referred to as "flare-ups") have been documented in the eastern Sierra Nevada batholith, age relationships in the western Sierra Nevada batholith are less well defined. The majority of studies of major intrusive suites in the Sierra Nevada batholith, with the exception of the Fine Gold intrusive suite (Lackey et al., 2012) in the western Sierra Nevada batholith, focus on high-elevation and well-exposed portions of the eastern Sierra Nevada batholith. Many western and northern Sierra Nevada batholith intrusions are "unassigned," and not part of a recognized intrusive suite. They also have limited geochronology, as does much of the southern Sierra Nevada batholith. Limited geochronology in areas where intrusive suites have not been defined may lead to interpretations of magmatic lulls in the Sierra Nevada batholith rather than a fundamental difference in magmatism. In addition, fewer Jurassic and Triassic intrusive suites have been identified, potentially due to the dissection of older parts of the batholith by Cretaceous intrusions, which complicates the connection of different plutons to suites representing single magmatic episodes. Figure 7 shows the ages of mafic bodies dated throughout the Sierra Nevada batholith relative to their distance from the left (southwestern) edge of Figure 1A, which is a line west of the Sierra Nevada batholith and subparallel to the trend of the batholith (trending ~20° azimuth; ages are given in Table 1). Mafic magmatism throughout the batholith follows this same trend that is recognized in the felsic batholith, with two main magmatic episodes in the eastern Sierra Nevada batholith but more temporally distributed magmatism throughout the western Sierra Nevada batholith. The story of episodic versus continuous magmatism and the relationship between mafic and felsic melts may be more nuanced in the western Sierra Nevada batholith, potentially owing to limited geochronological data for the western Sierra Nevada batholith compared to the eastern Sierra Nevada batholith.

Nonetheless, as we focus on the eastern Sierra Nevada batholith, the majority of mafic bodies in this study have ages similar to those of intermediate and felsic rocks in the same area, as they are located within and are coeval with designated intrusive suites in the eastern Sierra Nevada batholith, or are in contact with "unassigned" granitoids of similar age (Figs. 1, 3, and S1). The Cargyle Meadows mafic body (91.5 ± 1.4 Ma) is near the northern edge of the Mount Givens intrusive suite and similar in age to the oldest portions of this suite (98–90 Ma; Frazer et al., 2014). The Hidden Lakes (96–95 Ma; Lewis et al., 2021), Tamarack Lakes (94.6 ± 1.1 Ma), Lake Sabrina (91.1 ± 0.2 Ma; Coleman et al., 1995), and Green Lake (97.1 ± 3.3 Ma) mafic bodies are located within the John Muir intrusive suite and overlap its age within uncertainty (96–84 Ma; Davis et al., 2012). The Pine Creek diorite body (194.0 ± 2.6 Ma) is in contact with the granite of Chickenfoot Lake (191.8 ± 4.2 Ma; Lewis et al., 2021), which is not assigned to an intrusive suite and is equivalent to the Pine Creek age within uncertainty. The Mount Tom (145.1 ± 1.7 Ma), Tungsten Hills (148.3 ± 1.8 Ma), Bishop Creek (146.5 ± 1.4 Ma), and Shannon Canyon (168.2 ± 1.9 Ma) bodies are in contact with mapped lobes of the Tungsten Hills Quartz Monzonite (ca. 201–168 Ma). The Mount Alice (146.1 ± 1.6 Ma) and McMurry Meadows (152.3 ± 3.1 Ma) bodies are located within or on the margins of the Palisade Crest intrusive suite (ca. 158–170; Bateman, 1992a), and potentially represent late-stage intrusions of this magmatic episode. Furthermore, many of the ages from the Palisade Crest intrusive suite come from Rb/Sr whole-rock methods (Bateman, 1992a), so the Palisade Crest intrusive suite may require additional geochronology to better define its age. The Keough body (88.8 ± 1.3 Ma) intrudes the mapped leucogranite of Rawson Creek (97.2 ± 1.1 Ma), which is not assigned to an intrusive suite. The Armstrong Canyon body (91.5 ± 0.2 Ma; Coleman et al., 1995) is in contact with the coeval, unassigned granite of Goodale Mountain (92.6 ± 1.2 Ma; Coleman et al., 1995). The Onion Valley Complex (92.1 ± 0.3 Ma; Coleman et al., 1995) intrudes the Bullfrog pluton and Dragon pluton, both of which are unassigned and ca. 103 Ma (Chen and Moore, 1982). The mafic body at Black Canyon (157.2 ± 2.4 Ma) is intruded on nearly all sides by Late Cretaceous plutons but is in contact with the unassigned Mule Lake pluton (158.4 ± 1.5 Ma), which is similar in age to the mafic rocks. The Casa Diablo mafic body (100.2 ± 1.1 Ma) is the only example in this study that is not in contact with a granitoid of similar age, as it is a Late Cretaceous body that intruded into the Triassic quartz monzonite of Wheeler Crest (ca. 207 Ma; Stern et al., 1981). Due to its small size and elliptical shape, this mafic intrusion is likely a stock associated with magmatism in the early stages of the Late Cretaceous suites.

The intrusion of mafic melts into the upper crust within large intrusive suites or associated with unassigned granitoid plutons demonstrates

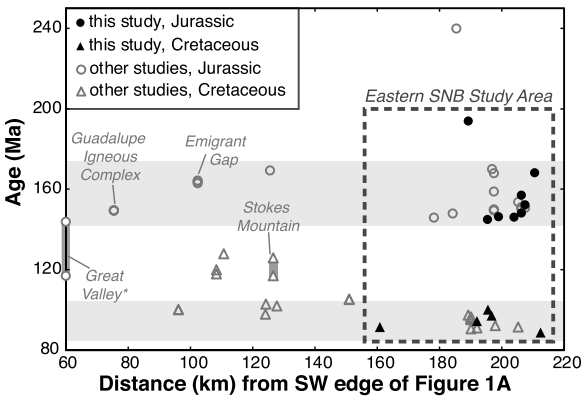

Figure 7. Distance of mafic bodies dated from the southwestern edge of Figure 1A, which trends near parallel to the Sierra Nevada batholith (SNB). Mafic body locations, ages, and references are given in Table 1. The Great Valley mafic intrusions were sampled in drill cores with a range of Cretaceous ages (indicated by the dark gray bar; Saleeby, 2007). The asterisk indicates that the Great Valley mafic intrusions are located west of Figure 1A. Two episodes of mafic magmatism in the eastern Sierra Nevada batholith are highlighted in gray; however, this trend is less prominent in the western Sierra Nevada batholith. Arc migration from west to east during the Cretaceous is apparent and was previously recognized in ages of Sierra Nevada batholith granitoids (Stern et al., 1981; Chen and Moore, 1982; Bateman, 1992a; Lackey et al., 2008; Ardill et al., 2018).

that voluminous felsic melt production is coeval with local mafic magmatism, which in turn is potentially driven by enhanced mantle melt flux. Migration of mantle melts to the base of the crust provides both juvenile basalts that can differentiate to form felsic crust, as well as heat to drive the melting of preexisting crust (e.g., Annen et al., 2006). Factors hypothesized to enhance felsic magma generation in arcs are debated and can be divided into mechanisms originating within the upper plate (i.e., continental crust) and external processes that enhance mantle melting. Proposed crustal-driven mechanisms include the melting of relaminated subducted sediments (Chapman et al., 2013), crustal over-thickening causing melting at the base of the arc (Ducea, 2001; DeCelles et al., 2009; Yang et al., 2020), and arc compression caused by subduction erosion and retroarc shortening (Ducea and Barton, 2007), all of which would increase crustal recycling. Processes resulting in enhanced mantle melting have also been proposed, such as changes to the subduction rate and slab angle, episodic fluxing of the mantle by slab fluids, slab tears and break-off, and mantle upwelling associated with the delamination of lower crustal cumulates (e.g., Decker et al., 2017; Martínez Ardila et al., 2019b; Cecil et al., 2021; Chapman et al., 2021). Our results indicate that mafic magmatism, likely mantle-derived, was enhanced during episodes of enhanced felsic plutonism in the eastern Sierra Nevada batholith, but they do not distinguish between different potential causes of episodic mantle melt production. Processes such as changes to the subduction angle, large-scale delamination or slab breakoff events, landward arc migration, or a combination of these events, may be capable of initiating widespread enhancements in mantle-melt generation (Martínez Ardila et al., 2019a; Chapman et al., 2021). Within the North American Cordillera, including the Coast Mountains and Peninsular Ranges batholiths (Gehrels et al., 2009; Premo et al., 2014; Cecil et al., 2011), extensive Late Cretaceous felsic magmatism is found during the same periods as in the Sierra Nevada batholith, which suggests that the processes affecting mantle melt generation are laterally extensive. Punctuated episodes of enhanced magmatism are also evident in arc batholiths that formed in other paleo-subduction zones, including the Median batholith in New Zealand (Schwartz et al., 2017), Peruvian Coastal batholith (Martínez Ardila et al., 2019a), Famatinian arc in South America (Otamendi et al., 2012), and the Gobi-Tianshan arc in Mongolia (Economos et al., 2012). Because the tectonic setting for magmatism in these continental arc batholiths is very similar to that of the Sierra Nevada batholith, it is likely that magmatism in these batholiths, and potentially other (paleo-)continental arcs worldwide, is controlled by processes similar to those of the Sierra Nevada batholith.

Enhanced supply of mantle-derived basalts driving magma generation resolves seemingly contradictory isotopic observations in Cordilleran batholiths that support either increased crustal or mantle input during periods of high magmatic flux. Elevated $\delta^{18}O$ values and decreases in $^{143}Nd/^{144}Nd$ ratios during the interpreted flare-up periods have been seen as evidence of increased crustal recycling (Ducea and Barton, 2007; Kirsch et al., 2016; Chapman et al., 2021; Klein et al., 2021). Yet, concurrent Sr and Hf isotope excursions are consistent with elevated mantle input and indicate that crustal assimilation is minimal and that the proportion of mantle-derived magmas to the arc is elevated over the same periods (Coleman et al., 1992; Coleman and Glazner, 1997; Attia et al., 2020). Zircon radiogenic Hf isotopic ratios yield equivocal results displaying both decreases during the construction of intrusive suites (e.g., Bear Valley intrusive suite; Klein et al., 2021) and dominantly mantle-like values during the Cretaceous and Jurassic magmatic episodes, as sampled in volcanic strata of the Ritter Range pendant (Attia et al., 2020). An increase in basalt flux into the arc is expected to generate magmas with mantle-like isotopic compositions in plutons generated by the fractionation of these mantle-derived melts. However, high mantle-melt input also acts as a heat supply and leads to an increase in crustal recycling into arc magmas, thus producing plutons with isotopic evidence of crustal assimilation. High mantle input does not preclude the incorporation of melts sourced from preexisting crust or relaminated schists; however, if the dominant heat source driving partial melting is provided by the intrusion of basalts, the volume of crustal melts contributing to granitoid formation cannot exceed the volume derived through differentiation of the basalts providing the heat (Dufek and Bergantz, 2005; Annen et al., 2006; Jagoutz and Klein, 2018; Moyen, 2020). Thus, both the heat and magmatic volumes provided by mantle-derived melts are required to drive batholith construction in the Sierra Nevada batholith.

CONCLUSIONS

Mafic magmas contribute heat and magmatic volumes needed to generate the dominantly felsic upper crust observed in arc batholiths, though the exposure of mafic intrusions is typically minor compared to that of far more voluminous granitoid plutons. Our survey uses mafic intrusions in the eastern Sierra Nevada batholith to assess the role of mafic magmas in the construction of this batholith. The compositional structure of the Sierra Nevada batholith is similar to that of other continental arc batholiths globally, so these findings may be applicable to other magmatic arcs. Gabbro through diorite intrusions are ubiquitous throughout the Sierra Nevada batholith upper crust, but their volume is small in comparison to the volume of intermediate and felsic plutons. We expanded on previous field observations, geochronology, and bulk-rock and mineral chemistry from 17 mafic intrusions in the eastern Sierra Nevada batholith to investigate their origin, as well as their temporal and compositional relationship to the felsic portions of the batholith. Our results support the following findings:

(1) Field relationships and new U-Pb zircon geochronology expand on existing evidence for contemporaneous mafic and felsic magmatism in the eastern Sierra Nevada batholith. The majority of mafic bodies are similar in age to one or more adjacent granitoid intrusions. Most mafic bodies fall spatially and temporally within recognized intrusive suites.

(2) Mineral compositions indicate that the parental melts of the majority of the eastern Sierra Nevada batholith mafic bodies have Mg#s of 50 ± 5. All of the mafic bodies studied require a stage of differentiation prior to upper crustal residence as they are not consistent with the crystallization of primitive melts of the mantle.

(3) Bulk-rock compositions and textures in some samples from the mafic bodies indicate that they are upper crustal cumulates, which indicates that crystal fractionation occurred within the upper crust. Compositional trends in major and minor elements are continuous with trends in the bulk of the granitoids of the Sierra Nevada batholith, which suggests a genetic link between the mafic and felsic end members of the batholith.

(4) Crustal thickness calculations of melt-like mafic samples and granitoids indicate crustal thickening of nearly 20 km from the Jurassic to the Late Cretaceous in the Sierra Nevada batholith.

ACKNOWLEDGMENTS

We are grateful to many field assistants over the years: J. Biasi, A. Trussell, M. Barickman, E. Sosa, S. Newall, B. Ratschbacher, and L. Lewis. We thank the Arizona Laserchron Center for assistance with LA-ICP-MS analyses. The geochronology was funded by an AGeS2 award to MJL, under National Science Foundation grant nos. EAR-1759200 and EAR-1759353. Any opinions, findings, and conclusions or recommendations expressed in this material are those of the author(s) and do not necessarily reflect the views of the National Science Foundation. Thank you to the AGeS program for its support. We thank Drew Coleman, Joshua Schwartz, and an anonymous reviewer of a previous version of this work for com-

ments that improved the manuscript. We are also thankful to Tom Sisson and an anonymous reviewer for their constructive reviews, and editors Robinson Cecil and Mihai Ducea for management and comments on this manuscript.

REFERENCES CITED

Ague, J.J., and Brimhall, G.H., 1988, Magmatic arc asymmetry and distribution of anomalous plutonic belts in the batholiths of California: Effects of assimilation, crustal thickness, and depth of crystallization: Geological Society of America Bulletin, v. 100, no. 6, p. 912–927, https://doi.org/10.1130/0016-7606(1988)100<0912:MAAADO>2.3.CO;2.

Almeev, R.R., Ariskin, A.A., Kimura, J.I., and Barmina, G.S., 2013, The role of polybaric crystallization in genesis of andesitic magmas: Phase equilibria simulations of the Bezymianny volcanic subseries: Journal of Volcanology and Geothermal Research, v. 263, p. 182–192, https://doi.org/10.1016/j.jvolgeores.2013.01.004.

Annen, C., and Sparks, R.S.J., 2002, Effects of repetitive emplacement of basaltic intrusions on thermal evolution and melt generation in the crust: Earth and Planetary Science Letters, v. 203, no. 3–4, p. 937–955, https://doi.org/10.1016/S0012-821X(02)00929-9.

Annen, C., Blundy, J., and Sparks, R., 2006, The genesis of intermediate and silicic magmas in deep crustal hot zones: Journal of Petrology, v. 47, no. 3, p. 505–539, https://doi.org/10.1093/petrology/egi084.

Ardill, K., Paterson, S., and Memeti, V., 2018, Spatiotemporal magmatic focusing in upper-mid crustal plutons of the Sierra Nevada arc: Earth and Planetary Science Letters, v. 498, p. 88–100, https://doi.org/10.1016/j.epsl.2018.06.023.

Armstrong, J.T., 1995, Citzaf-a package of correction programs for the quantitative electron microbeam X-ray analysis of thick polished materials, thin-films, and particles: Microbeam Analysis, v. 4, no. 3, p. 177–200.

Attia, S., Cottle, J.M., and Paterson, S.R., 2020, Erupted zircon record of continental crust formation during mantle driven arc flare-ups: Geology, v. 48, no. 5, p. 446–451, https://doi.org/10.1130/G46991.1.

Barth, A.P., Walker, J.D., Wooden, J.L., Riggs, N.R., and Schweickert, R.A., 2011, Birth of the Sierra Nevada magmatic arc: Early Mesozoic plutonism and volcanism in the east-central Sierra Nevada of California: Geosphere, v. 7, no. 4, p. 877–897, https://doi.org/10.1130/GES00661.1.

Bartley, J.M., Glazner, A.F., Coleman, D.S., Kylander-Clark, A., Mapes, R., Friedrich, A.M., and Till, A., 2007, Large Laramide dextral offset across Owens Valley, California, and its possible relation to tectonic unroofing of the southern Sierra Nevada, *in* Roeske, S.M., Till, A.B., Foster, D.A., and Sample, J.C., eds., Exhumation Associated with Continental Strike-Slip Fault Systems: Geological Society of America Special Paper 434, p. 129–148, https://doi.org/10.1130/2007.2434(07).

Bateman, P.C., 1965, Geology and tungsten mineralization of the Bishop district, California: U.S. Geological Survey Professional Paper 470.

Bateman, P.C., 1992a, Plutonism in the central part of the Sierra Nevada batholith, California: U.S. Geological Survey Professional Paper 1483.

Bateman, P.C., 1992b, Pre-Tertiary bedrock geologic map of the Mariposa 1° by 2° quadrangle, Sierra Nevada, California: U.S. Geological Survey IMAP 1960.

Bateman, P.C., and Chappell, B.W., 1979, Crystallization, fractionation, and solidification of the Tuolumne intrusive series, Yosemite National Park, California: Geological Society of America Bulletin, v. 90, no. 5, p. 465–482, https://doi.org/10.1130/0016-7606(1979)90<465:CFASOT>2.0.CO;2.

Bateman, P.C., and Eaton, J.P., 1967, Sierra Nevada Batholith: The batholith was generated within a synclinorium: Science, v. 158, no. 3807, p. 1407–1417, https://doi.org/10.1126/science.158.3807.1407.

Beattie, P., 1993, Olivine-melt and orthopyroxene-melt equilibria: Contributions to Mineralogy and Petrology, v. 115, no. 1, p. 103–111, https://doi.org/10.1007/BF00712982.

Blatter, D.L., Sisson, T.W., and Hankins, W.B., 2013, Crystallization of oxidized, moderately hydrous arc basalt at mid-to lower-crustal pressures: Implications for andesite genesis: Contributions to Mineralogy and Petrology, v. 166, no. 3, p. 861–886, https://doi.org/10.1007/s00410-013-0920-3.

Bucholz, C.E., and Spencer, C.J., 2019, Strongly peraluminous granites across the Archean–Proterozoic transition: Journal of Petrology, v. 60, no. 7, p. 1299–1348, https://doi.org/10.1093/petrology/egz033.

Cecil, M.R., Gehrels, G., Ducea, M.N., and Patchett, P.J., 2011, U-Pb-Hf characterization of the central Coast Mountains batholith: Implications for petrogenesis and crustal architecture: Lithosphere, v. 3, no. 4, p. 247–260, https://doi.org/10.1130/L134.1.

Cecil, M.R., et al., 2021, Mantle control on magmatic flare-ups in the southern Coast Mountains batholith, British Columbia: Geosphere, v. 17, no. 6, p. 2027–2041, https://doi.org/10.1130/GES02361.1.

Chapman, A.D., Saleeby, J.B., Wood, D.J., Piasecki, A., Kidder, S., Ducea, M.N., and Farley, K.A., 2012, Late Cretaceous gravitational collapse of the southern Sierra Nevada batholith, California: Geosphere, v. 8, no. 2, p. 314–341, https://doi.org/10.1130/GES00740.1.

Chapman, A.D., Saleeby, J.B., and Eiler, J., 2013, Slab flattening trigger for isotopic disturbance and magmatic flare-up in the southernmost Sierra Nevada batholith, California: Geology, v. 41, no. 9, p. 1007–1010, https://doi.org/10.1130/G34445.1.

Chapman, J.B., Ducea, M.N., DeCelles, P.G., and Profeta, L., 2015, Tracking changes in crustal thickness during orogenic evolution with Sr/Y: An example from the North American Cordillera: Geology, v. 43, no. 10, p. 919–922, https://doi.org/10.1130/G36996.1.

Chapman, J.B., Shields, J.E., Ducea, M.N., Paterson, S.R., Attia, S., and Ardill, K.E., 2021, The causes of continental arc flare ups and drivers of episodic magmatic activity in Cordilleran orogenic systems: Lithos, v. 398–399, https://doi.org/10.1016/j.lithos.2021.106307.

Chen, J.H., and Moore, J.G., 1979, Late Jurassic Independence dike swarm in eastern California: Geology, v. 7, no. 3, p. 129–133, https://doi.org/10.1130/0091-7613(1979)7<129:LJIDSI>2.0.CO;2.

Chen, J.H., and Moore, J.G., 1982, Uranium-lead isotopic ages from the Sierra Nevada batholith, California: Journal of Geophysical Research: Solid Earth, v. 87, no. B6, p. 4761–4784, https://doi.org/10.1029/JB087iB06p04761.

Clemens-Knott, D., 2016, Reconstructing the record of Jurassic arc magmatism, Kern Plateau, southern Sierra Nevada, CA: Geological Society of America Abstracts with Programs, v. 48, no. 4, https://doi.org/10.1130/abs/2016CD-274737.

Clemens-Knott, D., and Saleeby, J.B., 1999, Impinging ring dike complexes in the Sierra Nevada batholith, California: Roots of the Early Cretaceous volcanic arc: Geological Society of America Bulletin, v. 111, no. 4, p. 484–496, https://doi.org/10.1130/0016-7606(1999)111<0484:IRDCIT>2.3.CO;2.

Coleman, D., Glazner, A., Miller, J., Bradford, K., Frost, T., Joye, J., and Bachl, C., 1995, Exposure of a Late Cretaceous layered mafic-felsic magma system in the central Sierra Nevada Batholith, California: Contributions to Mineralogy and Petrology, v. 120, no. 2, p. 129–136, https://doi.org/10.1007/BF00287110.

Coleman, D.S., and Glazner, A.F., 1997, The Sierra Crest magmatic event: Rapid formation of juvenile crust during the Late Cretaceous in California: International Geology Review, v. 39, no. 9, p. 768–787, https://doi.org/10.1080/00206819709465302.

Coleman, D.S., Glazner, A.F., and Frost, T.P., 1992, Evidence from the Lamarck Granodiorite for rapid Late Cretaceous crust formation in California: Science, v. 258, no. 5090, p. 1924–1926, https://doi.org/10.1126/science.258.5090.1924.

Coleman, D.S., Carl, B.S., Glazner, A.F., and Bartley, J.M., 2000, Cretaceous dikes within the Jurassic Independence dike swarm in eastern California: Geological Society of America Bulletin, v. 112, no. 3, p. 504–511, https://doi.org/10.1130/0016-7606(2000)112<504:CDWTJI>2.0.CO;2.

Coleman, D.S., Gray, W., and Glazner, A.F., 2004, Rethinking the emplacement and evolution of zoned plutons: Geochronologic evidence for incremental assembly of the Tuolumne intrusive suite, California: Geology, v. 32, no. 5, p. 433–436, https://doi.org/10.1130/G20220.1.

Collins, W.J., Huang, H.Q., and Jiang, X., 2016, Water-fluxed crustal melting produces Cordilleran batholiths: Geology, v. 44, no. 2, p. 143–146, https://doi.org/10.1130/G37398.1.

Davis, J.W., Coleman, D.S., Gracely, J.T., Gaschnig, R., and Stearns, M., 2012, Magma accumulation rates and thermal histories of plutons of the Sierra Nevada batholith, CA: Contributions to Mineralogy and Petrology, v. 163, no. 3, p. 449–465, https://doi.org/10.1007/s00410-011-0683-7.

DeCelles, P.G., Ducea, M.N., Kapp, P., and Zandt, G., 2009, Cyclicity in Cordilleran orogenic systems: Nature Geoscience, v. 2, no. 4, p. 251–257, https://doi.org/10.1038/ngeo469.

Decker, M., Schwartz, J.J., Stowell, H.H., Klepeis, K.A., Tulloch, A.J., Kitajima, K., Valley, J.W., and Kylander-Clark, A.R.C., 2017, Slab-triggered arc flare-up in the Cretaceous Median Batholith and the growth of lower arc crust, Fiordland, New Zealand: Journal of Petrology, v. 58, no. 6, p. 1145–1171, https://doi.org/10.1093/petrology/egx049.

DePaolo, D.J., 1981, A neodymium and strontium isotopic study of the Mesozoic calc-alkaline granitic batholiths of the Sierra Nevada and Peninsular Ranges, California: Journal of Geophysical Research: Solid Earth, v. 86, no. B11, p. 10,470–10,488, https://doi.org/10.1029/JB086iB11p10470.

Dodge, F., Calk, L., and Kistler, R., 1986, Lower crustal xenoliths, Chinese Peak lava flow, central Sierra Nevada: Journal of Petrology, v. 27, no. 6, p. 1277–1304, https://doi.org/10.1093/petrology/27.6.1277.

Dodge, F., Lockwood, J., and Calk, L., 1988, Fragments of the mantle and crust from beneath the Sierra Nevada batholith: Xenoliths in a volcanic pipe near Big Creek, California: Geological Society of America Bulletin, v. 100, no. 6, p. 938–947, https://doi.org/10.1130/0016-7606(1988)100<0938:FOTMAC>2.3.CO;2.

Dorais, M.J., Whitney, J.A., and Roden, M.F., 1990, Origin of mafic enclaves in the Dinkey Creek pluton, central Sierra Nevada batholith, California: Journal of Petrology, v. 31, no. 4, p. 853–881, https://doi.org/10.1093/petrology/31.4.853.

Ducea, M.N., 2001, The California arc: Thick granitic batholiths, eclogitic residues, lithospheric-scale thrusting, and magmatic flare-ups: GSA Today, v. 11, no. 11, p. 4–10, https://doi.org/10.1130/1052-5173(2001)011<0004:TCATGB>2.0.CO;2.

Ducea, M.N., and Barton, M.D., 2007, Igniting flare-up events in Cordilleran arcs: Geology, v. 35, no. 11, p. 1047–1050, https://doi.org/10.1130/G23898A.1.

Dufek, J., and Bergantz, G.W., 2005, Lower crustal magma genesis and preservation: A stochastic framework for the evaluation of basalt–crust interaction: Journal of Petrology, v. 46, no. 11, p. 2167–2195, https://doi.org/10.1093/petrology/egi049.

Economos, R.C., Paterson, S.R., Said, L.O., Ducea, M.N., Anderson, J.L., and Padilla, A.J., 2012, Gobi-Tianshan connections: Field observations and isotopes from an Early Permian arc complex in southern Mongolia: Geological Society of America Bulletin, v. 124, no. 11–12, p. 1688–1701, https://doi.org/10.1130/B30324.1.

Elder, D., and Reichert, M., 2010, Region-wide GIS bedrock compilation mapping—An ArcSDE geodatabase Version 2.0: Digital dataset (agency internal publication): USDA Forest Service, Pacific Southwest Region 5, Vallejo, California.

Evernden, J.F., and Kistler, R.W., 1970, Chronology of emplacement of Mesozoic batholithic complexes in California and western Nevada: U.S. Geological Survey Professional Paper 623, 42 p., https://doi.org/10.3133/pp623.

Frazer, R., Coleman, D., and Mills, R., 2014, Zircon U-Pb geochronology of the Mount Givens Granodiorite, central Sierra Nevada, California: Implications for the genesis of large volumes of eruptible magma: Journal of Geophysical Research: Solid Earth, v. 119, p. 2907–2924, https://doi.org/10.1002/2013JB010716.

Frost, T., and Mattinson, J., 1988, Late Cretaceous U-Pb age of a mafic intrusion from the eastern Sierra Nevada, California: Isochron-West, v. 51, p. 15–18.

Frost, T., and Mattinson, J., 1993, Age and tectonic implications of mid-Mesozoic calc-alkalic hornblende-rich mafic plutonic rocks of the eastern Sierra Nevada, California: Isochron-West, v. 59, p. 11–16.

Frost, T.P., 1987, Sample localities, radiometric ages, descriptions, and major-and trace-element abundances of Late Jurassic mafic plutonic rocks, eastern Sierra Nevada, California: U.S. Geological Survey Open File Report 87-484, 33 p.

Frost, T.P., and Mahood, G.A., 1987, Field, chemical, and physical constraints on mafic-felsic magma interaction in the Lamarck Granodiorite, Sierra Nevada, California: Geological Society of America Bulletin, v. 99, no. 2, p. 272–291, https://doi.org/10.1130/0016-7606(1987)99<272:FCAPCO>2.0.CO;2.

Gaschnig, R.M., 2005, Cause, timing, and significance of brittle deformation in Little Lakes Valley, eastern Sierra Nevada, California [M.S. thesis]: Chapel Hill, North Carolina, University of North Carolina at Chapel Hill.

Gehrels, G., et al., 2009, U-Th-Pb geochronology of the Coast Mountains batholith in north-coastal British Columbia: Constraints on age and tectonic evolution: Geological Society of America Bulletin, v. 121, no. 9–10, p. 1341–1361, https://doi.org/10.1130/B26404.1.

Gehrels, G.E., Valencia, V.A., and Ruiz, J., 2008, Enhanced precision, accuracy, efficiency, and spatial resolution of U-Pb ages by laser ablation–multicollector–inductively coupled plasma–mass spectrometry: Geochemistry, Geophysics, Geosystems, v. 9, no. 3, https://doi.org/10.1029/2007GC001805.

Gevedon, M., 2013, Paired oxygen and hafnium isotopic analysis of zircon from gabbros: Identifying potential Mesozoic mantle heterogeneity in the Sierra Nevada arc [M.S. thesis]: Fullerton, California, California State University.

Gevedon, M., Lackey, J.S., and Barnes, J.D., 2021, Skarn fluid sources as indicators of timing of Cordilleran arc emergence and paleogeography in the southwestern United States: Geology, v. 49, no. 11, p. 1317–1321, https://doi.org/10.1130/G49005.1.

Ghiorso, M.S., and Sack, R.O., 1995, Chemical mass transfer in magmatic processes IV. A revised and internally consistent thermodynamic model for the interpolation and extrapolation of liquid-solid equilibria in magmatic systems at elevated temperatures and pressures: Contributions to Mineralogy and Petrology, v. 119, no. 2–3, p. 197–212, https://doi.org/10.1007/BF00307281.

Girty, G.H., Yoshinobu, A.S., Wracher, M.D., Girty, M.S., Bryan, K.A., Skinner, J.E., McNulty, B.A., and Bracchi, K.A., 1993, U-Pb zircon geochronology of the Emigrant Gap composite pluton, Northern Sierra Nevada, California: Implications for the Nevadan orogeny, *in* Dunn, G., and McDougall, K., eds., Mesozoic Paleogeography of the Western United States, II: Pacific Section, Society of Economic Paleontologists and Mineralogists (SEPM), v. 71, p. 323–332.

Glazner, A.F., Carl, B.S., Coleman, D.S., Miller, J.S., Bartley, J.M., Wright, J.E., and Shervais, J.W., 2008, Chemical variability and the composite nature of dikes from the Jurassic Independence dike swarm, eastern California, *in* Wright, J.E., and Shervais, J.W., eds., Ophiolites, Arcs, and Batholiths: A Tribute to Cliff Hopson: Geological Society of America Special Paper 438, p. 455–480, https://doi.org/10.1130/2008.2438(16).

Hamada, M., Okayama, Y., Kaneko, T., Yasuda, A., and Fujii, T., 2014, Polybaric crystallization differentiation of H_2O-saturated island arc low-K tholeiite magmas: A case study of the Izu-Oshima volcano in the Izu arc: Earth, Planets and Space, v. 66, p. 1–10, https://doi.org/10.1186/1880-5981-66-15.

Hildebrand, R.S., 2013, Mesozoic Assembly of the North American Cordillera: Geological Society of America Special Paper 495, 169 p., https://doi.org/10.1130/SPE495.

Hirt, W.H., 2007, Petrology of the Mount Whitney intrusive suite, eastern Sierra Nevada, California: Implications for the emplacement and differentiation of composite felsic intrusions: Geological Society of America Bulletin, v. 119, no. 9–10, p. 1185–1200, https://doi.org/10.1130/B26054.1.

Holland, J.E., Surpless, B., Smith, D.R., Loewy, S.L., and Lackey, J.S., 2013, Intrusive history and petrogenesis of the Ash Mountain Complex, Sierra Nevada batholith, California (USA): Geosphere, v. 9, no. 4, p. 691–717, https://doi.org/10.1130/GES00890.1.

Hopson, R.F., Hillhouse, J.W., and Howard, K.A., 2008, Dike orientations in the Late Jurassic Independence dike swarm and implications for vertical-axis tectonic rotations in eastern California, *in* Wright, J.E., and Shervais, J.W., eds., Ophiolites, Arcs, and Batholiths: A Tribute to Cliff Hopson: Geological Society of America Special Paper 438, p. 481–498, https://doi.org/10.1130/2008.2438(17).

Jagoutz, O., and Kelemen, P.B., 2015, Role of arc processes in the formation of continental crust: Annual Review of Earth and Planetary Sciences, v. 43, p. 363–404, https://doi.org/10.1146/annurev-earth-040809-152345.

Jagoutz, O., and Klein, B., 2018, On the importance of crystallization-differentiation for the generation of SiO_2-rich melts and the compositional build-up of arc (and continental) crust: American Journal of Science, v. 318, no. 1, p. 29–63, https://doi.org/10.2475/01.2018.03.

Jagoutz, O., and Schmidt, M.W., 2013, The composition of the foundered complement to the continental crust and a re-evaluation of fluxes in arcs: Earth and Planetary Science Letters, v. 371–372, p. 177–190, https://doi.org/10.1016/j.epsl.2013.03.051.

Jagoutz, O.E., 2010, Construction of the granitoid crust of an island arc. Part II: A quantitative petrogenetic model: Contributions to Mineralogy and Petrology, v. 160, no. 3, p. 359–381, https://doi.org/10.1007/s00410-009-0482-6.

Jagoutz, O.E., Burg, J.P., Hussain, S., Dawood, H., Pettke, T., Iizuka, T., and Maruyama, S., 2009, Construction of the granitoid crust of an island arc part I: Geochronological and geochemical constraints from the plutonic Kohistan (NW Pakistan): Contributions to Mineralogy and Petrology, v. 158, no. 6, p. 739–755, https://doi.org/10.1007/s00410-009-0408-3.

James, O.B., 1971, Origin and emplacement of the ultramafic rocks of the Emigrant Gap area, California: Journal of Petrology, v. 12, no. 3, p. 523–560, https://doi.org/10.1093/petrology/12.3.523.

Kirsch, M., Paterson, S.R., Wobbe, F., Ardila, A.M.M., Clausen, B.L., and Alasino, P.H., 2016, Temporal histories of Cordilleran continental arcs: Testing models for magmatic episodicity: The American Mineralogist, v. 101, no. 10, p. 2133–2154, https://doi.org/10.2138/am-2016-5718.

Kistler, R., Bateman, P., and Brannock, W., 1965, Isotopic ages of minerals from granitic rocks of the central Sierra Nevada and Inyo Mountains, California: Geological Society of America Bulletin, v. 76, no. 2, p. 155–164, https://doi.org/10.1130/0016-7606(1965)76[155:IAOMFG]2.0.CO;2.

Kistler, R.W., and Anderson, J.L., 1990, Two different lithosphere types in the Sierra Nevada, California: The nature and origin of Cordilleran magmatism, *in* Anderson, J.L., ed., The Nature and Origin of Cordilleran Magmatism: Geological Society of America Memoir 174, p. 271–282, https://doi.org/10.1130/MEM174-p271.

Kistler, R.W., and Peterman, Z.E., 1973, Variations in Sr, Rb, K, Na, and initial Sr^{87}/Sr^{86} in Mesozoic granitic rocks and intruded wall rocks in central California: Geological Society of America Bulletin, v. 84, no. 11, p. 3489–3512, https://doi.org/10.1130/0016-7606(1973)84<3489:VISRKN>2.0.CO;2.

Klein, B.Z., and Jagoutz, O., 2021, Construction of a transcrustal magma system: Building the Bear Valley intrusive suite, southern Sierra Nevada, California: Earth and Planetary Science Letters, v. 553, https://doi.org/10.1016/j.epsl.2020.116624.

Klein, B.Z., Jagoutz, O., and Ramezani, J., 2021, High-precision geochronology requires that ultrafast mantle-derived magmatic fluxes built the transcrustal Bear Valley intrusive suite, Sierra Nevada, California, USA: Geology, v. 49, no. 1, p. 106–110, https://doi.org/10.1130/G47952.1.

Lackey, J.S., Valley, J.W., Chen, J.H., and Stockli, D.F., 2008, Dynamic magma systems, crustal recycling, and alteration in the central Sierra Nevada batholith: The oxygen isotope record: Journal of Petrology, v. 49, no. 7, p. 1397–1426, https://doi.org/10.1093/petrology/egn030.

Lackey, J.S., Cecil, M.R., Windham, C.J., Frazer, R.E., Bindeman, I.N., and Gehrels, G.E., 2012, The Fine Gold intrusive suite: The roles of basement terranes and magma source development in the Early Cretaceous Sierra Nevada batholith: Geosphere, v. 8, no. 2, p. 292–313, https://doi.org/10.1130/GES00745.1.

Lee, C.T., Rudnick, R.L., and Brimhall, G.H., Jr., 2001, Deep lithospheric dynamics beneath the Sierra Nevada during the Mesozoic and Cenozoic as inferred from xenolith petrology: Geochemistry, Geophysics, Geosystems, v. 2, no. 12, https://doi.org/10.1029/2001GC000152.

Lee, C.T.A., Cheng, X., and Horodyskyj, U., 2006, The development and refinement of continental arcs by primary basaltic magmatism, garnet pyroxenite accumulation, basaltic recharge and delamination: Insights from the Sierra Nevada, California: Contributions to Mineralogy and Petrology, v. 151, no. 2, p. 222–242, https://doi.org/10.1007/s00410-005-0056-1.

Leopold, M.B., 2016, Structure, construction, and emplacement of the Late Cretaceous Sonora pass intrusive suite: Central Sierra Nevada batholith, California [M.S. thesis]: San Jose, California, San José State University, 99 p.

Lewis, M.J., Bucholz, C.E., and Jagoutz, O.E., 2021, Evidence for polybaric fractional crystallization in a continental arc: Hidden Lakes mafic complex, Sierra Nevada batholith, California: Contributions to Mineralogy and Petrology, v. 176, no. 11, p. 1–27, https://doi.org/10.1007/s00410-021-01844-y.

Mahan, K.H., Bartley, J.M., Coleman, D.S., Glazner, A.F., and Carl, B.S., 2003, Sheeted intrusion of the synkinematic McDoogle pluton, Sierra Nevada, California: Geological Society of America Bulletin, v. 115, no. 12, p. 1570–1582, https://doi.org/10.1130/B22083.1.

Martínez Ardila, A.M., Clausen, B.L., Memeti, V., and Paterson, S.R., 2019a, Source contamination, crustal assimilation, and magmatic recycling during three flare-up events in the Cretaceous Peruvian Coastal Batholith: An example from the Ica-Pisco plutons: Journal of South American Earth Sciences, v. 95, https://doi.org/10.1016/j.jsames.2019.102300.

Martínez Ardila, A.M., Paterson, S.R., Memeti, V., Parada, M.A., and Molina, P.G., 2019b, Mantle driven Cretaceous flare-ups in Cordilleran arcs: Lithos, v. 326–327, p. 19–27, https://doi.org/10.1016/j.lithos.2018.12.007.

Marxer, F., Ulmer, P., and Müntener, O., 2022, Polybaric fractional crystallisation of arc magmas: An experimental study simulating trans-crustal magmatic systems: Contributions to Mineralogy and Petrology, v. 177, no. 1, p. 3, https://doi.org/10.1007/s00410-021-01856-8.

Mattinson, J.M., 2010, Analysis of the relative decay constants of ^{235}U and ^{238}U by multi-step CA-TIMS measurements of closed-system natural zircon samples: Chemical Geology, v. 275, no. 3–4, p. 186–198, https://doi.org/10.1016/j.chemgeo.2010.05.007.

Mayo, E.B., 1941, Deformation in the interval Mt. Lyell-Mt. Whitney, California: Geological Society of America Bulletin, v. 52, no. 7, p. 1001–1084, https://doi.org/10.1130/GSAB-52-1001.

Melekhova, E., Blundy, J., Robertson, R., and Humphreys, M.C., 2015, Experimental evidence for polybaric differentiation of primitive arc basalt beneath St. Vincent, Lesser Antilles: Journal of Petrology, v. 56, no. 1, p. 161–192, https://doi.org/10.1093/petrology/egu074.

Moore, J.G., 1963, Geology of the Mount Pinchot quadrangle, southern Sierra Nevada, California: U.S. Geological Survey Bulletin 1130, scale 1:62,500.

Moore, J.G., and Sisson, T.W., 1987, Geologic map of the Triple Divide Peak quadrangle, Tulare County, California: U.S. Geological Survey Bulletin 1636, scale 1:62,500.

Moyen, J.F., 2020, Granites and crustal heat budget, *in* Janoušek, V., Bonin, B., Collins, W.J., Farina, F., and Bowden, P., eds., Post-Archean Granitic Rocks: Petrogenetic Processes and Tectonic Environments: Geological Society, London, Special Publication 491, p. 77–100, https://doi.org/10.1144/SP491-2018-148.

Mukhopadhyay, B., and Manton, W., 1994, Upper-mantle fragments from beneath the Sierra Nevada Batholith: Partial fusion, fractional crystallization, and metasomatism in a subduction related ancient lithosphere: Journal of Petrology, v. 35, no. 5, p. 1417–1450, https://doi.org/10.1093/petrology/35.5.1417.

Müntener, O., and Ulmer, P., 2018, Arc crust formation and differentiation constrained by experimental petrology: American Journal of Science, v. 318, no. 1, p. 64–89, https://doi.org/10.2475/01.2018.04.

Nandedkar, R.H., Ulmer, P., and Müntener, O., 2014, Fractional crystallization of primitive, hydrous arc magmas: An experimental study at 0.7 GPa: Contributions to Mineralogy and Petrology, v. 167, no. 6, p. 1–27, https://doi.org/10.1007/s00410-014-1015-5.

Otamendi, J.E., Ducea, M.N., Tibaldi, A.M., Bergantz, G.W., de la Rosa, J.D., and Vujovich, G.I., 2009, Generation of tonalitic and dioritic magmas by coupled partial melting of gabbroic and metasedimentary rocks within the deep crust of the Famatinian magmatic arc, Argentina: Journal of Petrology, v. 50, no. 5, p. 841–873, https://doi.org/10.1093/petrology/egp022.

Otamendi, J.E., Ducea, M.N., and Bergantz, G.W., 2012, Geological, petrological and geochemical evidence for progressive construction of an arc crustal section, Sierra de Valle Fértil, Famatinian Arc, Argentina: Journal of Petrology, v. 53, no. 4, p. 761–800, https://doi.org/10.1093/petrology/egr079.

Paces, J.B., and Miller, J.D., Jr., 1993, Precise U-Pb ages of Duluth complex and related mafic intrusions, northeastern Minnesota: Geochronological insights to physical, petrogenetic, paleomagnetic, and tectonomagmatic processes associated with the 1.1 Ga midcontinent rift system: Journal of Geophysical Research: Solid Earth, v. 98, no. B8, p. 13,997–14,013, https://doi.org/10.1029/93JB01159.

Paterson, S.R., and Ducea, M.N., 2015, Arc magmatic tempos: Gathering the evidence: Elements, v. 11, no. 2, p. 91–98, https://doi.org/10.2113/gselements.11.2.91.

Pickett, D.A., and Saleeby, J.B., 1993, Thermobarometric constraints on the depth of exposure and conditions of plutonism and metamorphism at deep levels of the Sierra Nevada batholith, Tehachapi Mountains, California: Journal of Geophysical Research: Solid Earth, v. 98, no. B1, p. 609–629, https://doi.org/10.1029/92JB01889.

Pickett, D.A., and Saleeby, J.B., 1994, Nd, Sr, and Pb isotopic characteristics of Cretaceous intrusive rocks from deep levels of the Sierra Nevada batholith, Tehachapi Mountains, California: Contributions to Mineralogy and Petrology, v. 118, no. 2, p. 198–215, https://doi.org/10.1007/BF01052869.

Porter, J.P., 2013, Source, emplacement, and evolution of the Morgan Creek pluton, Sierra Nevada batholith, California, USA [M.S. thesis]: Salt Lake City, Utah, University of Utah.

Premo, W.R., Morton, D.M., Wooden, J.L., Fanning, C.M., and Miller, F., 2014, U-Pb zircon geochronology of plutonism in the northern Peninsular Ranges batholith, southern California: Implications for the Late Cretaceous tectonic evolution of southern California, *in* Morton, D.M., and Miller, F.K., eds., Peninsular Ranges Batholith, Baja California and Southern California: Geological Society of America Memoir 211, p. 145–180, https://doi.org/10.1130/2014.1211(04).

Profeta, L., Ducea, M.N., Chapman, J.B., Paterson, S.R., Gonzales, S.M.H., Kirsch, M., Petrescu, L., and DeCelles, P.G., 2015, Quantifying crustal thickness over time in magmatic arcs: Scientific Reports, v. 5, no. 1, https://doi.org/10.1038/srep17786.

Pullen, A., Ibáñez-Mejia, M., Gehrels, G.E., Giesler, D., and Pecha, M., 2018, Optimization of a laser ablation-single collector-inductively coupled plasma-mass spectrometer (Thermo Element 2) for accurate, precise, and efficient zircon U-Th-Pb geochronology: Geochemistry, Geophysics, Geosystems, v. 19, no. 10, p. 3689–3705, https://doi.org/10.1029/2018GC007889.

Putirka, K.D., Canchola, J., Rash, J., Smith, O., Torrez, G., Paterson, S.R., and Ducea, M.N., 2014, Pluton assembly and the genesis of granitic magmas: Insights from the GIC pluton in cross section, Sierra Nevada Batholith, California: The American Mineralogist, v. 99, no. 7, p. 1284–1303, https://doi.org/10.2138/am.2014.4564.

Ratajeski, K., Glazner, A.F., and Miller, B.V., 2001, Geology and geochemistry of mafic to felsic plutonic rocks in the Cretaceous intrusive suite of Yosemite Valley, California: Geological Society of America Bulletin, v. 113, no. 11, p. 1486–1502, https://doi.org/10.1130/0016-7606(2001)113<1486:GAGOMT>2.0.CO;2.

Ratschbacher, B.C., Keller, C.B., Schoene, B., Paterson, S.R., Anderson, J.L., Okaya, D., Putirka, K., and Lippoldt, R., 2018, A new workflow to assess emplacement duration and melt residence time of compositionally diverse magmas emplaced in a sub-volcanic reservoir: Journal of Petrology, v. 59, no. 9, p. 1787–1809, https://doi.org/10.1093/petrology/egy079.

Reid, J.B., Jr., Evans, O.C., and Fates, D.G., 1983, Magma mixing in granitic rocks of the central Sierra Nevada, California: Earth and Planetary Science Letters, v. 66, p. 243–261, https://doi.org/10.1016/0012-821X(83)90139-5.

Rezeau, H., Klein, B.Z., and Jagoutz, O., 2021, Mixing dry and wet magmas in the lower crust of a continental arc: New petrological insights from the Bear Valley intrusive suite, southern Sierra Nevada, California: Contributions to Mineralogy and Petrology, v. 176, no. 9, p. 1–25, https://doi.org/10.1007/s00410-021-01832-2.

Ross, D.C., 1985, Mafic: Gneissic complex (batholithic root?) in the southernmost Sierra Nevada, California: Geology, v. 13, no. 4, p. 288–291, https://doi.org/10.1130/0091-7613(1985)13<288:MGCBRI>2.0.CO;2.

Ross, D.C., 1989, The metamorphic and plutonic rocks of the southernmost Sierra Nevada, California, and their tectonic framework: U.S. Geological Survey Professional Paper 1381, https://doi.org/10.3133/pp1381.

Rudnick, R.L., and Gao, S., 2003, Composition of the continental crust, *in* Holland, H.D., and Turekian, K.K., eds., Treatise on Geochemistry: The Mantle and Core: Amsterdam, Elsevier, v. 3, p. 1–64.

Saleeby, J., 2007, The western extent of the Sierra Nevada batholith in the Great Valley basement and its significance in underlying mantle dynamics: Abstract T31E-02 presented at 2007 Fall Meeting, AGU, San Francisco, California, 10–14 December.

Saleeby, J., and Dunne, G., 2015, Temporal and tectonic relations of early Mesozoic arc magmatism, southern Sierra Nevada, California: Late Jurassic margin of Laurasia—A record of faulting accommodating plate rotation, *in* Anderson, T.H., Didenko, A.N., Johnson, C.L., Khanchuk, A.I., and MacDonald, J.H., Jr., eds., Late Jurassic Margin of Laurasia—A Record of Faulting Accommodating Plate Rotation: Geological Society of America Special Paper 513, p. 223–268, https://doi.org/10.1130/2015.2513(05).

Saleeby, J., and Sharp, W., 1980, Chronology of the structural and petrologic development of the southwest Sierra Nevada foothills, California: Summary: Geological Society of America Bulletin, v. 91, no. 6, p. 317–320, https://doi.org/10.1130/0016-7606(1980)91<317:COTSAP>2.0.CO;2.

Saleeby, J., Ducea, M.N., Busby, C., Nadin, E., Wetmore, P.H., Wright, J., and Shervais, J., 2008, Chronology of pluton emplacement and regional deformation in the southern Sierra Nevada batholith, California, *in* Wright, J.E., and Shervais, J.W., eds., Ophiolites, Arcs, and Batholiths: A Tribute to Cliff Hopson: Geological Society of America Special Paper 438, p. 397–427, https://doi.org/10.1130/2008.2438(14).

Saleeby, J.B., Shaw, H.F., Niemeyer, S., Moores, E.M., and Edelman, S.H., 1989, U/Pb, Sm/Nd and Rb/Sr geochronological and isotopic study of northern Sierra Nevada ophiolitic assemblages, California: Contributions to Mineralogy and Petrology, v. 102, no. 2, p. 205–220, https://doi.org/10.1007/BF00375341.

Sams, D.B., and Saleeby, J.B., 1988, Geology and petrotectonic significance of crystalline rocks of the southernmost Sierra Nevada, California, *in* Ernst, W.G., ed., Metamorphism and Crustal Evolution of the Western United States: Englewood Cliffs, New Jersey, Prentice Hall, Rubey v. 7, p. 866–893.

Sawka, W.N., 1988, REE and trace element variations in accessory minerals and hornblende from the strongly zoned McMurry Meadows Pluton, California: Earth and Environmental Science Transactions of the Royal Society of Edinburgh, v. 79, no. 2–3, p. 157–168, https://doi.org/10.1017/S0263593300014188.

Sawka, W.N., Chappell, B.W., and Kistler, R.W., 1990, Granitoid compositional zoning by side-wall boundary layer differentiation: Evidence from the Palisade Crest intrusive suite, central Sierra Nevada, California: Journal of Petrology, v. 31, no. 3, p. 519–553, https://doi.org/10.1093/petrology/31.3.519.

Schwartz, J.J., Klepeis, K.A., Sadorski, J.F., Stowell, H.H., Tulloch, A.J., and Coble, M.A., 2017, The tempo of continental arc construction in the Mesozoic Median Batholith, Fiordland, New Zealand: Lithosphere, v. 9, no. 3, p. 343–365, https://doi.org/10.1130/L610.1.

Sisson, T., and Grove, T., 1993, Experimental investigations of the role of H_2O in calc-alkaline differentiation and subduction zone magmatism: Contributions to Mineralogy and Petrology, v. 113, no. 2, p. 143–166, https://doi.org/10.1007/BF00283225.

Sisson, T., and Moore, J., 2010, Osa Creek gabbro-granite ring complex, Sierra Nevada, CA, by degassing-driven subsidence of mafic-magmatic sheets: Abstract V11C-2294 presented at 2010 Fall Meeting, AGU, San Francisco, California, 13–17 December.

Sisson, T., Grove, T., and Coleman, D., 1996, Hornblende gabbro sill complex at Onion Valley, California, and a mixing origin for the Sierra Nevada batholith: Contributions to Mineralogy and Petrology, v. 126, no. 1–2, p. 81–108, https://doi.org/10.1007/s004100050237.

Sisson, T.W., and Kelemen, P.B., 2018, Near-solidus melts of MORB+ 4 wt% H_2O at 0.8–2.8 GPa applied to issues of subduction magmatism and continent formation: Contributions to Mineralogy and Petrology, v. 173, no. 9, p. 1–23, https://doi.org/10.1007/s00410-018-1494-x.

Sisson, T.W., and Moore, J.G., 1984, Geology of Giant Forest–Lodgepole area, Sequoia National Park, California: U.S. Geological Survey Open-File Report 84-245, 13 p., https://doi.org/10.3133/ofr84254.

Sisson, T.W., and Moore, J.G., 2013, Geologic map of southwestern Sequoia National Park, Tulare County, California: U.S. Geological Survey Open File Report 1096, scale 1:24,000.

Sisson, T.W., Ratajeski, K., Hankins, W.B., and Glazner, A.F., 2005, Voluminous granitic magmas from common basaltic sources: Contributions to Mineralogy and Petrology, v. 148, no. 6, p. 635–661, https://doi.org/10.1007/s00410-004-0632-9.

Stern, T.W., Bateman, P.C., Morgan, B.A., Newell, M.F., and Peck, D.L., 1981, Isotopic U-Pb ages of zircon from the granitoids of the central Sierra Nevada, California: U.S. Geological Survey Professional Paper 1185, https://doi.org/10.3133/pp1185.

Tobisch, O.T., Fiske, R.S., Saleeby, J.B., Holt, E., and Sorensen, S.S., 2000, Steep tilting of metavolcanic rocks by multiple mechanisms, central Sierra Nevada, California: Geological Society of America Bulletin, v. 112, no. 7, p. 1043–1058, https://doi.org/10.1130/0016-7606(2000)112<1043:STOMRB>2.0.CO;2.

Turner, S.J., and Langmuir, C.H., 2022, A quantitative framework for global variations in arc geochemistry: Earth and Planetary Science Letters, v. 584, https://doi.org/10.1016/j.epsl.2022.117411.

Turner, S.J., Langmuir, C.H., Katz, R.F., Dungan, M.A., and Escrig, S., 2016, Parental arc magma compositions dominantly controlled by mantle-wedge thermal structure: Nature Geoscience, v. 9, no. 10, p. 772–776, https://doi.org/10.1038/ngeo2788.

Vermeesch, P., 2018, IsoplotR: A free and open toolbox for geochronology: Geoscience Frontiers, v. 9, no. 5, p. 1479–1493, https://doi.org/10.1016/j.gsf.2018.04.001.

Wenner, J.M., and Coleman, D.S., 2004, Magma mixing and Cretaceous crustal growth: Geology and geochemistry of granites in the central Sierra Nevada Batholith, California: International Geology Review, v. 46, no. 10, p. 880–903, https://doi.org/10.2747/0020-6814.46.10.880.

Yang, J., Cao, W., Gordon, S.M., and Chu, X., 2020, Does underthrusting crust feed magmatic flare-ups in continental arcs?: Geochemistry, Geophysics, Geosystems, v. 21, no. 11, https://doi.org/10.1029/2020GC009152.

Zeng, L., Saleeby, J.B., and Ducea, M., 2005, Geochemical characteristics of crustal anatexis during the formation of migmatite at the Southern Sierra Nevada, California: Contributions to Mineralogy and Petrology, v. 150, no. 4, p. 386–402, https://doi.org/10.1007/s00410-005-0010-2.

Science Editor: Mihai Ducea
Associate Editor: Robinson Cecil

Manuscript Received 20 June 2022
Revised Manuscript Received 21 April 2023
Manuscript Accepted 19 May 2023

Printed in the USA